BRL R 1953

BRL

AD AD35250

DEC NOV 1996
CIRCULATING COPY

REPORT NO. 1953

NUMERICAL SOLUTION OF THREE SOLID PROPELLANT COMBUSTION MODELS DURING A GUN PRESSURE TRANSIENT

Douglas E. Kooker
Carl W. Nelson

January 1977

Approved for public release; distribution unlimited.

USA BALLISTIC RESEARCH LABORATORIES
ABERDEEN PROVING GROUND, MARYLAND

Destroy this report when it is no longer needed.
Do not return it to the originator.

Secondary distribution of this report by originating or sponsoring activity is prohibited.

Additional copies of this report may be obtained from the National Technical Information Service, U.S. Department of Commerce, Springfield, Virginia 22151.

The findings in this report are not to be construed as an official Department of the Army position, unless so designated by other authorized documents.

UNCLASSIFIED

SECURITY CLASSIFICATION OF THIS PAGE *(When Data Entered)*

REPORT DOCUMENTATION PAGE		READ INSTRUCTIONS BEFORE COMPLETING FORM
1. REPORT NUMBER BRL REPORT NO. 1953	2. GOVT ACCESSION NO.	3. RECIPIENT'S CATALOG NUMBER
4. TITLE *(and Subtitle)* Numerical Solution of Three Solid Propellant Combustion Models During a Gun Pressure Transient		5. TYPE OF REPORT & PERIOD COVERED BRL Report 6. PERFORMING ORG. REPORT NUMBER
7. AUTHOR(s) Douglas E. Kooker Carl W. Nelson		8. CONTRACT OR GRANT NUMBER(s)
9. PERFORMING ORGANIZATION NAME AND ADDRESS USA Ballistic Research Laboratory Aberdeen Proving Ground, MD 21005		10. PROGRAM ELEMENT, PROJECT, TASK AREA & WORK UNIT NUMBERS 1T161102AH53
11. CONTROLLING OFFICE NAME AND ADDRESS USA Materiel Development and Readiness Command 5001 Eisenhower Avenue Alexandria, VA 22333		12. REPORT DATE January 1977 13. NUMBER OF PAGES 56
14. MONITORING AGENCY NAME & ADDRESS*(if different from Controlling Office)*		15. SECURITY CLASS. *(of this report)* Unclassified 15a. DECLASSIFICATION/DOWNGRADING SCHEDULE

16. DISTRIBUTION STATEMENT *(of this Report)*

Approved for public release; distribution unlimited.

17. DISTRIBUTION STATEMENT *(of the abstract entered in Block 20, if different from Report)*

18. SUPPLEMENTARY NOTES

19. KEY WORDS *(Continue on reverse side if necessary and identify by block number)*

Transient Solid Propellant Combustion; Thermal-Wave Combustion Models; Numerical Solution; Burning Rate Runaway; Gun Pressure Transient.

ssv/4589

20. ABSTRACT *(Continue on reverse side if necessary and identify by block number)* All current gun interior ballistics computer programs rely on, and are sensitive to, the steady state burning rate "law", $r=ap^n$. It is not clear that this is a valid representation in a highly transient pressure environment. To estimate possible dynamic effects, numerical solutions for three thermal-wave combustion models (KTSS, Levine/Culick, Kooker/Zinn) are obtained for a series of example cases where the imposed pressure variation at the edge of the flame zone is prescribed by an experimental pressure-time history from the 105mm Gun M68. The results obtained with

DD FORM 1 JAN 73 1473 EDITION OF 1 NOV 65 IS OBSOLETE

UNCLASSIFIED

SECURITY CLASSIFICATION OF THIS PAGE *(When Data Entered)*

several different numerical solution methods indicate that (1) at low pressure (early time) the instantaneous propellant burning rate can be much greater than ap^n; while at high pressure the burning rate returns asymptotically to ap^n, and (2) burning rate "runaway" is a numerical difficulty and is not a solution to the combustion models. The effect of dynamic burning rate on closed-bomb measurements is estimated numerically with a simple model.

TABLE OF CONTENTS

This page Left Intentionally Blank

LIST OF FIGURES

LIST OF FIGURES
(Continued)

NOMENCLATURE

a	constant in burning rate law, $r = ap^n$
A	$E(1 - T_\infty/T_{so})$, [n-d]
c_s, c_p	specific heat of solid and gas, respectively
E; E_s	$E_s/R_o T_{so}$, [n-d]; activation energy of surface reaction
G	defined in Eq. (1c), [n-d]
H	$\overline{Q}_s/c_s(T_{so} - T_\infty)$, [n-d]
k_s, k_g	thermal conductivity of solid and gas, respectively
K_1, K_2	defined in Eqs. (5) and (6), respectively
m	exponent in Eq. (9)
$\dot{m}$	mass flow rate = $\rho_s r$ [see Eq. (2a)]
n	pressure exponent in burning rate law, $r = ap^n$
n_s	pressure exponent in Eq. (13)
p; P	pressure; p/p_o [n-d]
q_g	heat flux to interface from gas-phase flame
Q_s, Q_f	heat release per unit mass for surface reaction and flame reaction, respectively
r; R	surface regression rate; r/r_o, [n-d]
R_s	R computed from a steady state expression, usually $R_s = P^n$, [n-d]
R_o	universal gas constant
t	time
T; T_{so}; T_∞	temperature; initial surface temperature; cold-solid temperature
x	distance coordinate, normal to propellant surface

NOMENCLATURE

Z	$\frac{c_p}{c_s}\left(\frac{T_{so}}{T_{so} - T_\infty}\right)\Lambda_o^2$, [n-d]
α	$k_s/\rho_s c_s$, thermal diffusivity
$\hat{\beta}$	reaction order [see Eq. (15)]
β	defined in Eq. (28)
η	$x(r_o/\alpha)$, [n-d]
Θ; Θ_s	$\frac{T - T_\infty}{T_{so} - T_\infty}$, [n-d]; nondimensional surface temperature
Λ_o^2	$k_g Q_f \omega_o/(\dot{m}_o^2 c_p^2 T_{so})$, [n-d]
ρ_s, ρ_g	density of solid and gas, respectively
τ	$t(r_o^2/\alpha)$, [n-d]
Φ	defined in Eq. (7)
ω	mass production rate
superscript	$\bar{}$ at steady state
subscript	o initial conditions

I. INTRODUCTION

Theoretical efforts to predict gun interior ballistics are faced with the formidable problem of analyzing a three-dimensional, viscous, heat conducting, chemically reacting, two-phase flow field. Because of these difficulties, recent work has concentrated on a simpler, one-dimensional, inviscid model which then requires correlation formulas to determine drag losses and heat transfer rates between the gas and solid particles. Equally important is an 'a priori' description of the behavior of the solid propellant burning rate. All current gun interior ballistics computer programs (1-6) rely on, and are sensitive to, the steady state burning rate "law", $r = ap^n$, possibly modified with an erosive burning contribution. However, this relationship is assumed to be valid in a highly transient pressure environment. If the burning rate is not properly represented, a successful gun-code prediction of maximum pressure and muzzle velocity may indicate that other adjustable parameters in the interior ballistics theory have artificially compensated.

---

[1] *Gough, P. S. and Zwarts, F. J., "Theoretical Model for Ignition of Gun Propellant," Report SRC-R-67, Space Research Corp. (December 1972); also Gough, P. S., "Fundamental Investigation of the Interior Ballistics of Guns," Report SRC-R-74, Space Research Corp. (August 1974).*

[2] *Krier, H., Van Tassell, W., Rajan, S., and VerShaw, J. T., "Model of Gun Propellant Flame Spreading and Combustion," BRL-CR-147 March , AD #918842L; also Krier, H., "Predictions of Flamespreading and Pressure Wave Propagation in Propellant Beds," AAE 75-6, University of Illinois (July 1975).*

[3] *Kuo, K., Vichnevetsky, R., and Summerfield, M., "Theory of Flame Front Propagation in Porous Propellant Charges Under Confinement," AIAA Journal, Vol 11, No. 3, pp 444-451 (April 1973).*

[4] *Fisher, E. B., and Trippe, A. P., "Development of a Basis for Acceptance of Continuously Produced Propellant," Report VQ-55163-D-1, Calspan Corp. (November 1973).*

[5] *East, J. L., and McClure, D. R., "Projectile Motion Predicted by a Solid/Gas Flow Interior Ballistic Model," 10th JANNAF Combustion Meeting, CPIA Publication 243 (August 1973).*

[6] *Baer, P. G., and Frankle, J. M., "The Simulation of Interior Ballistic Performance of Guns by Digital Computer Program," BRL Report 1183 (December 1962), AD #299980.*

Experimental verification of the instantaneous propellant burning rate during a rapid pressure change is a difficult task and, at the present time, is unavailable. Similarly, the time-dependent numerical solution of a comprehensive solid propellant combustion model which includes solid and gas-phase finite-rate chemical reactions has yet to be accomplished. An alternative is to examine the thermal-wave combustion theories (based on the quasi-steady flame assumption) which were originally developed for the study of combustion instability and/or extinguishment in solid propellant rocket engines. It is the purpose of this report to investigate the behavior of three such combustion models in a rapidly increasing pressure field typical of a large-caliber gun. The three models selected are:

1. KTSS (Krier, Tien, Sirignano, Summerfield) - Ref. 7.

2. Levine/Culick - Ref. 8.

3. Kooker/Zinn - Ref. 9.

The primary objective is to obtain the numerical solution for instantaneous propellant burning rate for a series of example cases where the imposed pressure variation at the edge of the flame zone is prescribed by an experimental pressure-time history from the 105mm Gun M68. These results can then be compared to the steady state expression, $r = ap^n$. A secondary objective is to evaluate the capabilities of four different numerical integration schemes which are used to generate the time-dependent solution to these solid propellant combustion models.

II. ANALYSIS

A. Derivation of Combustion Models

The derivation of each of the three models is based on a common set of simplifying assumptions. It is assumed that (1) the solid propellant combustion process can be described in a single spatial dimension, (2) the unburned propellant is homogeneous, incompressible, and inert, (3) the solid is converted into gas by a global pyrolysis reaction which occurs at an infinitesimally thin interface, and (4) the gas-phase flame

---

[7] *Krier, H., T'ien, J. S., Sirignano, W. A., and Summerfield, M., "Nonsteady Burning Phenomena of Solid Propellants: Theory and Experiments," AIAA Journal, Vol. 6, No. 2, pp 278-285 (February 1968).*

[8] *Levine, J. N., and Culick, F. E. C., "Nonlinear Analysis of Solid Rocket Combustion Instability," AFRPL-TR-74-45 (October 1974).*

[9] *Kooker, D. E., and Zinn, B. T., "Numerical Investigation of Nonlinear Axial Instabilities in Solid Rocket Motors," BRL-CR-141 (March 1974), AD #776954, see also AIAA Paper 73-1298.*

is quasi-steady and remains anchored to the interface. As a direct result of these assumptions, all three models, when written for the coordinate system shown in Fig. 1, reduce to the following initial/boundary value problem describing the thermal-wave in the unburned solid propellant:

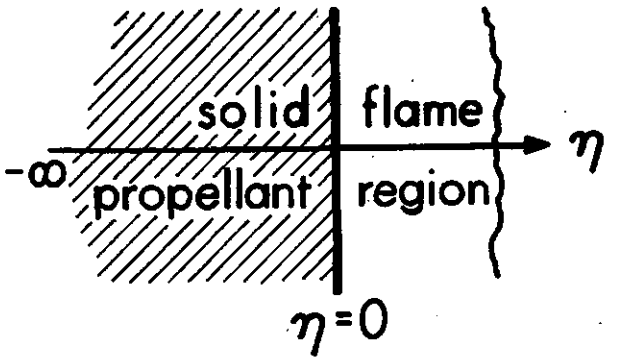

Figure 1 - Combustion Model Configuration

$$\Theta_\tau + R\Theta_\eta - \Theta_{\eta\eta} = 0 \qquad (-\infty < \eta \leq 0) \qquad (1)$$

initial condition

$$\Theta(\eta, 0) = e^{R\eta} \qquad (a)$$

boundary conditions

$$\Theta(-\infty, \tau) = 0 \qquad (b)$$

$$\Theta_\eta(0, \tau) = G\,(\Theta_s, R, P) \qquad (c)$$

$$\text{with } R = R(\Theta_s) \qquad (d)$$

where the particular form of G and R depends on the model in question. The quasi-steady flame assumption is incompatible with a proper description of the ignition event. Hence, the initial condition in the present application is taken to be the thermal-wave corresponding to an assumed steady-state burning rate. Equation (1b) of the boundary conditions enforces the cold-solid temperature at infinity, while Eq. (1c) is the result of an energy balance at the interface and includes the contribution of the gas-phase flame. The point of departure of the three models is the flame analysis and the postulated global pyrolysis reaction [Eq. (1d)].

When the low-velocity flame zone is assumed to be quasi-steady and one-dimensional, the equations of global continuity and momentum yield the almost trivial results,

$$\rho_g u_g = \rho_s r \equiv \dot{m} = \dot{m}(t) \qquad \text{(a)}$$

(2)

$$p = p(t). \qquad \text{(b)}$$

If the coupling with the species continuity equations is essentially ignored, the energy equation can be written in the form,

$$\dot{m} c_p \frac{dT}{dx} - \frac{d}{dx}\left(k_g \frac{dT}{dx}\right) = Q_f \omega \qquad (3)$$

where the right-hand side is the product of the heat released in the flame reaction(s) and the mass production rate of product species. The gradient boundary condition [Eq. (1c)] is a statement of the energy balance across the interface, x = 0, which can be written symbolically as

$$\left\{\begin{matrix}\text{heat flux into} \\ \text{solid propellant}\end{matrix}\right\} = \left\{\begin{matrix}\text{heat released in} \\ \text{surface reaction}\end{matrix}\right\} + \left\{\begin{matrix}\text{heat flux from} \\ \text{gas-phase flame}\end{matrix}\right\} . \qquad (4)$$

The "heat feedback" from the flame zone follows from the integral of Eq. (3), evaluated at the interface. Before the integration can be carried out, the spatial distribution of $Q_f\omega$ must be specified 'a priori'.

If the problem were posed correctly, the spatial distribution in question could easily be computed after obtaining the simultaneous solution of the energy equation and the species continuity equations. To assume the distribution of $Q_f\omega$ is known beforehand implies, in effect, that the solution has already been determined. Without resolving this contradiction, all three models employ the distribution,

$$Q_f\omega = \begin{cases} K_1, \text{ a constant} & 0 \le x \le x_f \\ 0 & x > x_f \end{cases} \qquad (5)$$

where x_f is the location of the edge of the flame zone. Another possibility would be

$$Q_f\omega = K_2\, \delta(x - x_f) \qquad (6)$$

where δ is the Dirac delta function. Obviously, in both cases, the "constant" K will change with time. It is sometimes claimed that integrating the energy equation under the constraint of Eq. (5) means that the flame analysis approximates a diffusion-controlled process,

whereas use of Eq. (6) (flame-sheet) approximates a chemical kinetic rate-controlled process. On this basis alone, the analysis which follows from Eq. (5) is said to apply to a composite propellant while the analysis following from Eq. (6) should apply to a double-base propellant. Considering the complexity of the actual solid propellant combustion process and the degree of simplicity and approximation involved in the one-dimensional models, it is felt that such a distinction is highly speculative. With due caution, the present analysis will assume the three models based on Eq. (5) represent the combustion of a triple-base propellant (M30) and interpret the results as possible trends.

The different form of the gradient boundary condition [Eq. (1c)] in each model can be traced to the method of evaluating K_1 in Eq. (5) after obtaining the integral of Eq. (3). In the KTSS model, when the characteristic combustion time is assumed to be a function of pressure alone, the integral of the energy equation leads to the conclusion that,

$$q_g = \Phi(p)/r \tag{7}$$

where q_g is the heat feedback from the gas-phase flame to the interface. $\Phi(p)$ is determined by assuming its functional dependence on pressure in the unsteady environment is the same as during steady state combustion, i.e., $\Phi(p) = \bar{r}\,\bar{q}_g$. The final result for the gradient boundary condition is (see Ref. 7 for details)

$$\theta_\eta(0,\tau) = RH + [P^{2n}\,(P^{n/m} - H)]/R \tag{8}$$

where $$R = \theta_s^{\,m}. \tag{9}$$

The power law dependence of R on surface temperature is used as an approximation to an Arrhenius reaction rate. The appearance of the pressure exponent "n" in Eq. (8) is the result of assuming that the steady state burning rate of the propellant is $\bar{r} = a\bar{p}^n$. Thus, if the pressure is held constant, the time-dependent model will predict a value of burning rate identical to this steady state law when all transient portions of the solution have died away. Of course, for a given value of pressure in an arbitrary time-dependent situation, the heat feedback from the gas-phase flame will not necessarily equal its steady state value at that pressure.

In the Levine/Culick model, the value of K_1 (and its dependence on pressure) is also determined without specifying the actual reaction scheme in the flame zone. Combining the steady-state temperature gradient in the solid at $x = 0$, the integral of Eq. (3) evaluated at $x = 0$, and the steady-state energy balance at the interface yields an expression for $\bar{\omega}$, viz.

$$\bar{\omega} = \frac{c_p}{Q_f k_s} \bar{m}^2 \left[c_s(\bar{T}_s - T_\infty) - \bar{Q}_s\right] . \tag{10}$$

By assuming that

$$\bar{m} = \rho_s a \bar{p}^n = B_s \bar{p}^{n_s} \exp\left(-E_s/R_o \bar{T}_s\right) \tag{11}$$

allows $\bar{m}$ and $\bar{T}_s$ to be eliminated from Eq. (10), leaving only the pressure dependence of $\bar{\omega}$. Then in the spirit of the quasi-steady flame assumption, the equation governing ω is found by replacing the steady state value of pressure with its instantaneous value. After considerable algebra (see Ref. 8), the final result for the gradient boundary condition is

$$\Theta_\eta(o,\tau) = R\left[H + (\Theta_s - 1)\left(1 - \frac{c_p}{c_s}\right)\right] + P^{2n}\left\{(1 - H) + \frac{c_p}{c_s}\frac{E}{A}\left[\frac{1}{1 + \frac{n_s - n}{E}\ln P} - 1\right]\right\} / R \tag{12}$$

where

$$R = P^{n_s} \exp\left[\frac{A(\Theta_s - 1)}{1 + \frac{A}{E}(\Theta_s - 1)}\right] . \tag{13}$$

Although somewhat disguised, Eq. (13) is the unsteady equivalent to the Arrhenius expression in Eq. (11); for all computations shown in the present paper, $n_s \equiv 0$. Similar to Ref. 7, the Levine/Culick model will also predict a value of burning rate identical to $a\bar{p}^n$ when the pressure is held constant and the transient portion of the solution has vanished.

In the Kooker/Zinn model, the flame region is assumed to be controlled by the simple one-step global reaction,

$$\text{Oxidizer} + \text{Fuel} \rightarrow \text{Products} \tag{14}$$

which implies

$$\omega \sim p^{\hat{\beta}} . \tag{15}$$

Although Eq. (14) is a global reaction as opposed to an elementary one, it is not improbable that $\hat{\beta}$, the "reaction order", could be 2 as used in Ref. 9. The present computations also employed the value 1.7. Under the assumption that the reaction occurs at a known flame temperature

and that the reaction order is specified, the integral of Eq. (3) leads to the result,

$$\Theta_\eta(0,\tau) = R[H + (\Theta_s - 1)(1 - \frac{c_p}{c_s})] + Z \frac{p^{\hat{\beta}}}{R} \qquad (16)$$

with R given by Eq. (13) when $n_s = 0$. The unknown multiplicative constant associated with Eq. (15) is determined by the interface energy balance at the initial condition, i.e.,

$$Z = 1 - H \qquad (17)$$

where the reference state in the nondimensionalization is taken to be the given initial conditions. Since a particular burning rate law has not been used in the derivation of Eq. (16), it is of interest to compute the pressure dependence of the steady burning rate inherent in the model. The example in Fig. 2 (based on the propellant parameters of Table 1) shows the results of constant pressure calculations for several values of pressure (hence the symbols in Fig. 2), assuming $\beta = 2$. The plots of $\ln R_s$ vs. $\ln P$ are not straight lines, but gentle curves concave upward. For lower values of surface heat release ($H \leq 0.7$ in this example) the curvature is slight; thus the model closely approximates $\bar{r} = a\bar{p}^n$. For larger values of H, the curvature is more pronounced; hence the model predicts a substantial increase in burning rate "exponent" with increasing pressure. In this example, both computations ($H = 0.70$ and 0.90) were unrealistically forced through the same initial conditions. This is responsible for the prediction that the larger value of H leads to a lower overall burning rate. However, the important point is that a very simple flame model can predict an increase in burning rate exponent with increasing pressure as observed experimentally for double and triple-base propellants.

B. Numerical Solution Methods

Predictions of the time-dependent burning rate for each combustion model require the solution to Eq. (1) using the appropriate interface boundary condition [Eq. (8) for KTSS; Eq. (12) for Levine/Culick; Eq. (16) for Kooker/Zinn]. An exact analytical solution is not possible since the primary equation and the boundary conditions are coupled and nonlinear. Because of the potential difficulty introduced by the nonlinearity, the present study examined four different numerical solution techniques, each of which has been used in previous investigations to solve combustion problems of this type. The objective is to see if the desired solution is independent of the method used to obtain it.

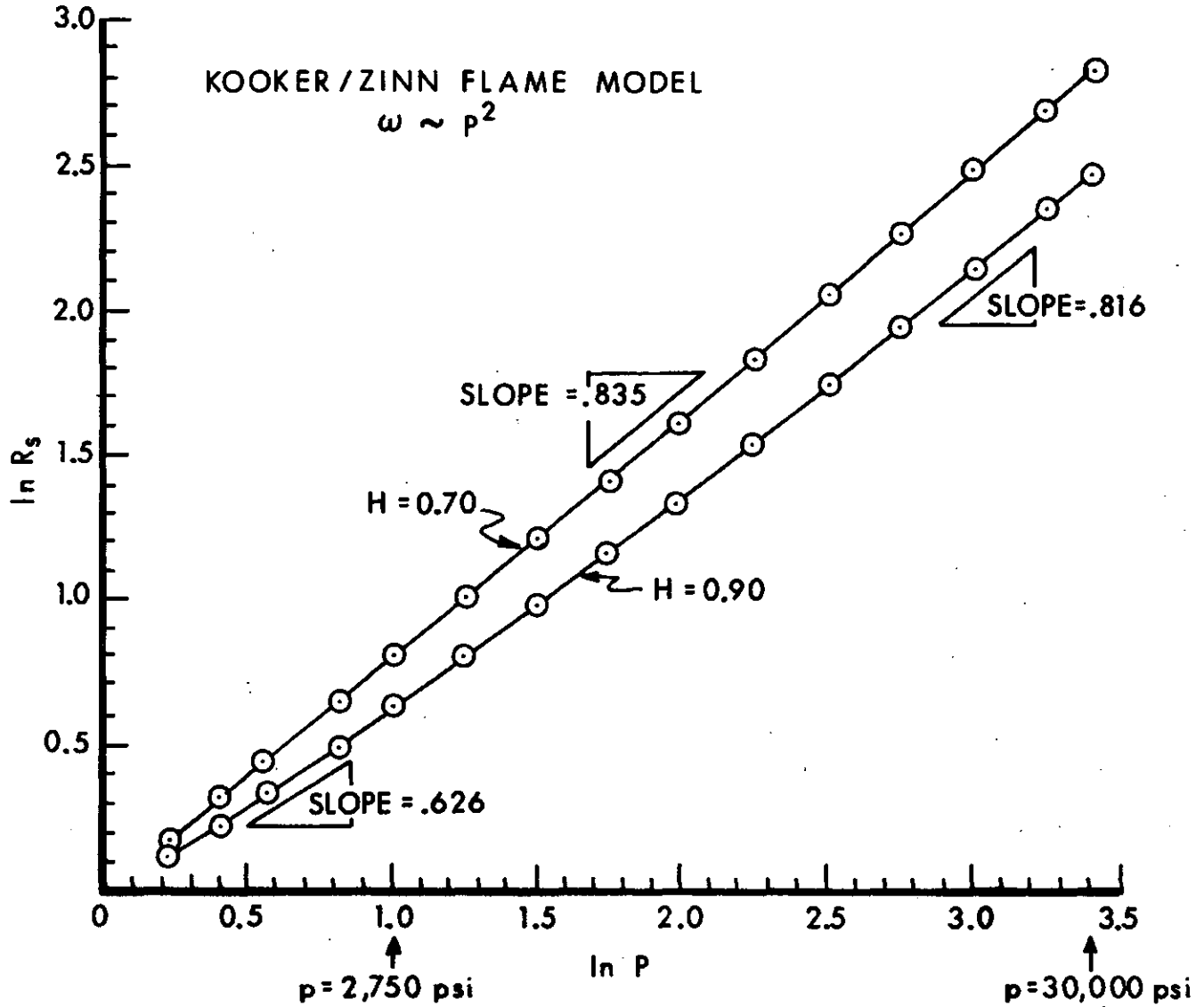

Figure 2. Steady State Burning Rate Predicted by Kooker/Zinn Model

Each numerical technique is expressed in the following notation. The superscripts n and n+1 refer to the current time level (where the solution is known) and the new time level, respectively. The subscripts j-1, j, j+1 refer to an arbitrary interior mesh point, j, and its two adjacent neighbors. For reasons to be discussed below, the mesh point distribution is non-uniform and hence $\Delta\eta_j \equiv \eta_j - \eta_{j-1}$ and $\Delta\eta_{j+1} \equiv \eta_{j+1} - \eta_j$ are not necessarily equal. For convenience, define

$$D\Theta_j \equiv \frac{\Delta\eta_j{}^2\Theta_{j+1} + (\Delta\eta^2{}_{j+1} - \Delta\eta^2{}_j)\,\Theta_j - \Delta\eta^2{}_{j+1}\,\Theta_{j-1}}{\Delta\eta_j\Delta\eta_{j+1}(\Delta\eta_j + \Delta\eta_{j+1})} \tag{18}$$

$$\cong \Theta_\eta \text{ at point } j,$$

$$DD\Theta_j \equiv 2\frac{\Delta\eta_{j+1}(\Theta_{j-1} - \Theta_j) + \Delta\eta_j(\Theta_{j+1} - \Theta_j)}{\Delta\eta_j\Delta\eta_{j+1}(\Delta\eta_j + \Delta\eta_{j+1})} \tag{19}$$

$$\cong \Theta_{\eta\eta} \text{ at point } j.$$

Then the four numerical techniques when applied to Eq. (1) can be written as,

(A) Explicit $[0(\Delta\tau, \Delta\eta^2{}_{max})$, stable for $\Delta\tau \leq \frac{1}{2}\Delta\eta^2{}_{min}]$

$$\frac{\Theta_j{}^{n+1} - \Theta_j{}^n}{\Delta\tau} + R^n\,(D\Theta_j{}^n) - DD\Theta_j{}^n = 0\,. \tag{20}$$

(B) Full Implicit $[0(\Delta\tau, \Delta\eta^2{}_{max})$, stable for any $\Delta\tau]$

$$\frac{\Theta_j{}^{n+1} - \Theta_j{}^n}{\Delta\tau} + R^{n+1}\,(D\Theta_j{}^{n+1}) - DD\Theta_j{}^{n+1} = 0\,. \tag{21}$$

(C) Crank-Nicolson Implicit $[0(\Delta\tau^2, \Delta\eta^2{}_{max})$, stable for any $\Delta\tau]$

$$\frac{\Theta_j{}^{n+1} - \Theta_j{}^n}{\Delta\tau} + \frac{1}{2}\Big\{ R^{n+1}\,(D\Theta_j{}^{n+1}) - DD\Theta_j{}^{n+1} + R^n(D\Theta_j{}^n) - DD\Theta_j{}^n \Big\} = 0\,. \tag{22}$$

(D) Invariant Imbedding Implicit $[0(\Delta\tau, \Delta\eta^2{}_{max})$ stable for any $\Delta\tau]$

See Appendix.

The coupling between the unknowns at j-1, j, and j+1 in Methods (B) and (C) leads to a tridiagonal matrix which is inverted with the standard Thomas Algorithm.

All the methods generate a finite difference equation (FDE) which is only an approximation to the true partial differential equation (PDE). The relationship between the two is based on Taylor series expansions and, using Method (B) as an example, can be written as,

$$FDE = PDE - \frac{\Delta\tau}{2}\Theta_{\tau\tau} + [R\Delta\eta_j\Delta\eta_{j+1} + 2(\Delta\eta_j - \Delta\eta_{j+1})](\Theta_{\eta\eta\eta}/6)$$

$$+ [R\Delta\eta_j\Delta\eta_{j+1}(\Delta\eta_{j+1} - \Delta\eta_j) - 2(\Delta\eta_j^2 - \Delta\eta_j\Delta\eta_{j+1} + \Delta\eta_{j+1}^2)]$$

$$(\Theta_{\eta\eta\eta}/24) \; . \qquad (23)$$

For equally-spaced mesh points, this reduces to the more familiar form,

$$FDE = PDE - \frac{\Delta\tau}{2}\Theta_{\tau\tau} + (2R\Theta_{\eta\eta\eta} - \Theta_{\eta\eta\eta})(\Delta\eta^2/12) \; . \qquad (24)$$

Based on Eq. (24), the formal order of accuracy is $O(\Delta\tau)$ and $O(\Delta\eta^2)$. However, unless the derivative terms are uniformly small, the formal argument can be misleading. Since the present combustion problem involves a thermal profile which may have very steep gradients near the interface, the spatial mesh must be closely spaced in this region (i.e., $\Delta\eta << 1$). Otherwise the truncation error will swamp the desired solution. Although no single mesh system will be optimal for all problems, Method (D) was used to determine a 231 grid point system [21 points, $-0.01 \leq \eta \leq 0$; 30 points, $-0.10 \leq \eta < -0.01$; 50 points, $-2.00 \leq \eta < -0.10$; 130 points, $-15.00 \leq \eta < -2.00$] such that the numerical solution for an extreme combustion problem was independent of further rearrangement and additional points.

The problem of nonlinearity must also be treated with care. Each numerical method effectively linearizes Eq. (1) in some manner. Furthermore the interface boundary condition, which must be applied at the new time level n+1, is a nonlinear function of the surface temperature at n+1. This requires an iteration procedure where the integration of Eq. (1) and the application of the boundary condition are updated cyclically. Convergence is assumed when the difference between the R used in Eq. (1) and the R which follows from the boundary condition is less than a specified tolerance (in this study, normally 10^{-8} using double precision computation). A crucial point concerning the size of the time step $\Delta\tau$ enters here. Although Methods (B) through (D) are

theoretically stable for an unrestricted time step, the iteration procedure is not. For those combustion problems where the surface temperature is changing rapidly with time, the time step must be appropriately restricted to keep the numerical solution from diverging. No mathematical proof is offered to support this conclusion. However, in the present investigation, the time step was continuously monitored and appropriately reduced if the number of cycles required for convergence of the iteration exceeded five.

C. Model Equation

The limiting accuracy of the numerical solution computed by Methods (A) through (D) can be estimated with an example denoted as the model equation. An exact analytical solution is available (see p. 389, Ref. 10) since both the equation and the boundary conditions are linear. Using the present notation, this system can be written as

$$\Theta_\tau + R\Theta_\eta - \Theta_{\eta\eta} = 0 \qquad [\tau \geq \tau_o,\ -\infty < \eta \leq 0] \tag{25}$$

initial condition

$$\Theta(\eta, \tau_o) = \Theta_o(\eta) \tag{a}$$

boundary conditions

$$\Theta(-\infty, \tau) = 0 \tag{b}$$

$$\Theta_\eta(0,\tau) = H\left[\Theta(0,\tau) + \frac{T_\infty}{T_{so} - T_\infty}\right] \tag{c}$$

where R and H are constants.

The example plotted in Fig. 3, with R=4.0, H=5.0, and τ_o=0.01 is viewed as a reasonable test of the methods even though it simulates a very large surface heating rate. The predicted numerical solution, based on the same grid mesh system used in the combustion problems, and the exact solution are indistinguishable on the scale of Fig. 3. The maximum error occurs at the surface η=0, and was within 1% for Method (D). Furthermore, using Method (D), the magnitude of the error at a given time level decreased as the size of the time step $\Delta\tau$ decreased. Method (A) may be equally accurate for this linear problem but the diffusion stability restriction on the time step is so small that the method is not competitive economically. For this reason, it was eliminated. For Methods (B) and (C), the maximum surface temperature error was within 2%, but the expected convergence as the time step was decreased did not always materialize. This can be traced to errors in the tridiagonal matrix inversion used by both Methods (B) and (C). Using a uniform mesh system as an example, the diagonal element of the matrix is given by

---

[10] *Carslaw, H. S., and Jaeger, J. C., Conduction of Heat in Solids, Oxford Press, 2nd edition (1959).*

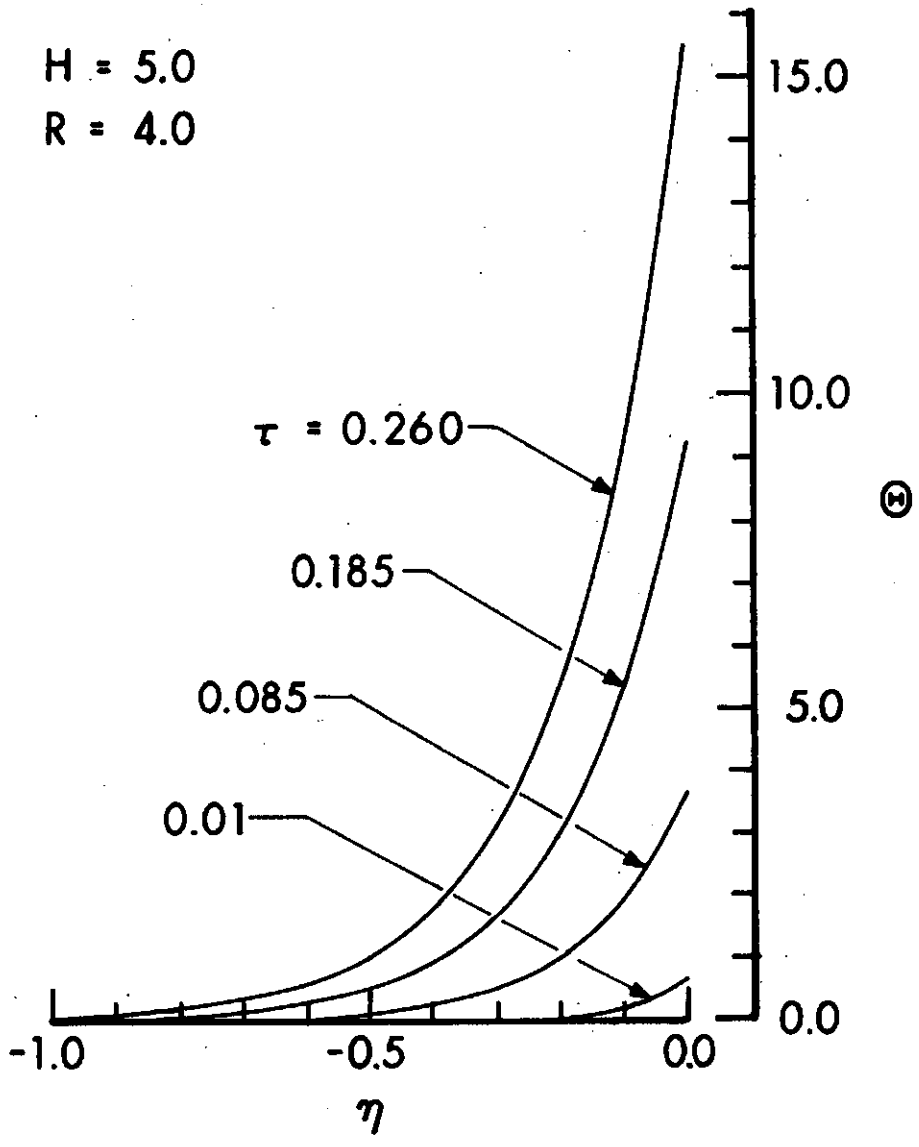

Figure 3. Solution to Model Equation, Eq. (25)

$$1 + \frac{2\Delta\tau}{\Delta\eta^2} \tag{26}$$

while the off-diagonal elements are

$$\frac{R\Delta\tau}{2\Delta\eta} \pm \frac{\Delta\tau}{\Delta\eta^2} \quad . \tag{27}$$

For time steps at or below the diffusion stability limit and with $R << 2/\Delta\eta$, diagonal dominance is assured. However, when using large time steps and nonlinear spacing (variable $\Delta\eta$), the absolute value of the diagonal term can change by orders of magnitude from one corner of the matrix to the other. This can create the same type of errors in the matrix inversion process as does loss of diagonal dominance. These errors can easily overpower the temporal truncation error in the finite difference equation, leading to the result that a decrease in $\Delta\tau$ does not produce the expected increase in accuracy. For the example shown in Fig. 3, however, the loss in accuracy is minimal.

On the basis of the linear model equation, it is concluded that Methods (B) through (D) yield nearly equal results with acceptable accuracy. The results from the linear model equation are not intended to be conclusive proof of accuracy for the combustion models to follow, but rather an estimate of the expected lower error bound. It should be stressed that the influence of the nonlinearity in the three combustion models has not been assessed in this exercise.

III. RESULTS

A. Burning Rate Response to a Sudden Compression

The purpose of this investigation is to compute the burning rate response to a rapidly increasing pressure field which simulates the gun combustion chamber environment. A similar problem is posed in Ref. 7 where one area of concern is the behavior of a rocket engine during a sudden compression. Several numerical computations in Ref. 7 are based on the pressure profile shown in Fig. 4, which is given by

$$P(\tau) = 1.0 + \Delta P \, [1.0 - \exp(-\beta\tau)] \, . \tag{28}$$

When $\Delta P = 2.5$ and $\beta = 1.0$, this expression approximates an experimental test run reported in Ref. 7. Equation (28) is not a good representation of a typical gun pressure time-history. However, it is relevant to the gun problem if viewed as a large amplitude pressure wave suddenly passing over a propellant grain which is burning at steady state. Such a situation could conceivably develop during a malfunction. For this reason, any results which follow from Eq. (28) are of interest to the

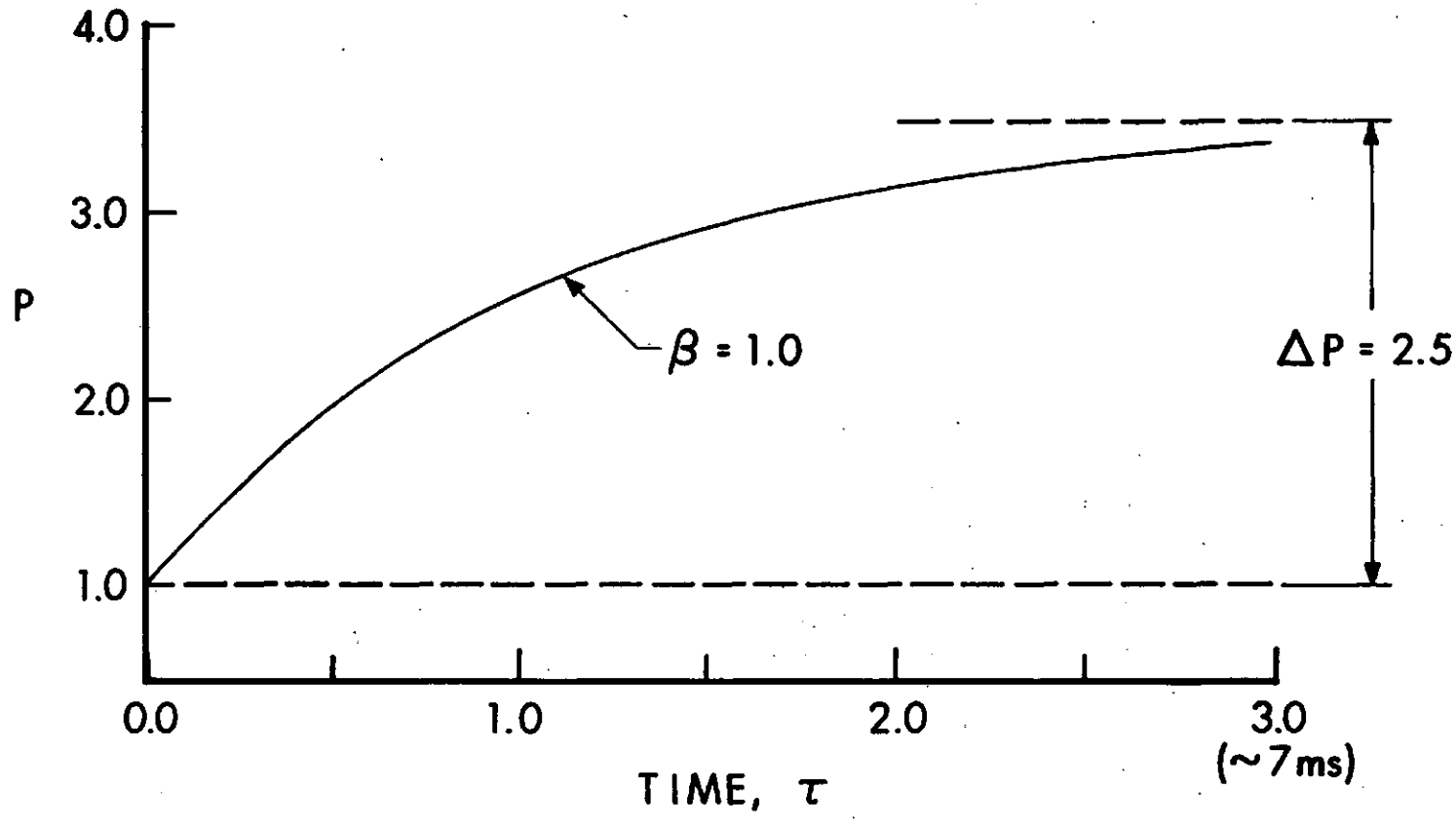

Figure 4. KTSS Exponential Pressure Profile

present analysis. A set of computations showing the sensitivity of the KTSS model to changes in the value of surface heat release (H) is reproduced here as Fig. 5 (see Fig. 9 in Ref. 7). The unbounded burning rate predicted for H = 0.80 is one of several calculations used as evidence of "intrinsic burning rate instability" or "runaway". A similar runaway condition was reported in Ref. 8 as the result of a sinusoidal pressure oscillation.

Because of the adverse influence that burning rate runaway would have in a gun system, the decision was made to examine each model in detail to determine the cause of the unbounded result and when it might occur. A first step was to use Method (D) to recompute the KTSS results for H = 0.80 shown in Fig. 5. The recomputed results are shown in Fig. 6; no runaway condition is indicated and the burning rate returns to the same value as H = 0.75 at a nondimensional time of approximately 1.2. Further computations of this case, however, showed that Method (D) will also predict a divergent solution if the time step restriction imposed by the iteration procedure is removed or a sufficient number of mesh points near the propellant interface are eliminated.

To see if "runaway" exists under more extreme conditions, the value of surface heat release (H) was increased to 0.90 and the response to the same exponential pressure profile was computed. The results (Method D) shown in Fig. 7 contain sharp finite-amplitude "spikes", similar to those reported in Ref. 9. An important difference, however, is that the burning rate response in Fig. 7 is due to a monotonically increasing pressure field and not a sinusoidal pressure oscillation. The behavior of the thermal wave during a spike is the same as that discussed on page 24 pertaining to the results in Fig. 14. Although these results appear unconventional and may suggest that the combustion model is oversimplified, an extensive rechecking of the numerical computation indicates that Fig. 7 is the actual solution to the equations. To determine if the finite-amplitude spikes are model dependent, the Kooker/Zinn combustion model (with H = 0.9 and $\hat{\beta}$ = 1.7) was driven by the same monotonically increasing pressure field given by Eq. (28). The numerical solution (Method D) shown in Fig. 8, exhibits the same qualitative behavior as the KTSS model. A strong resemblance to this type of burning rate phenomenon has been reported in the Russian literature (Ref. 11) for a related problem. Reference 11 considers "gas-less" combustion of a solid propellant (or explosive) which burns by means of a single, in-depth, irreversible, condensed-phase reaction. The equations solved are identical to those used by Bradley (Ref. 12, with a = 1) in his study of radiant ignition of a reactive solid. Since the model does

---

[11] *Shkadinskii, K. G., Khaikin, B. I., and Merzhanov, A. G., "Propagation of a Pulsating Exothermic Reaction Front in the Condensed Phase," Fizika Goreniya i Varyva, Vol 7, No. 1, pp 19-28 (1971).*

[12] *Bradley, H. H., Jr., "Theory of Ignition of a Reactive Solid by Constant Energy Flux," Comb Sci & Tech, Vol 2, pp 11-20 (1970).*

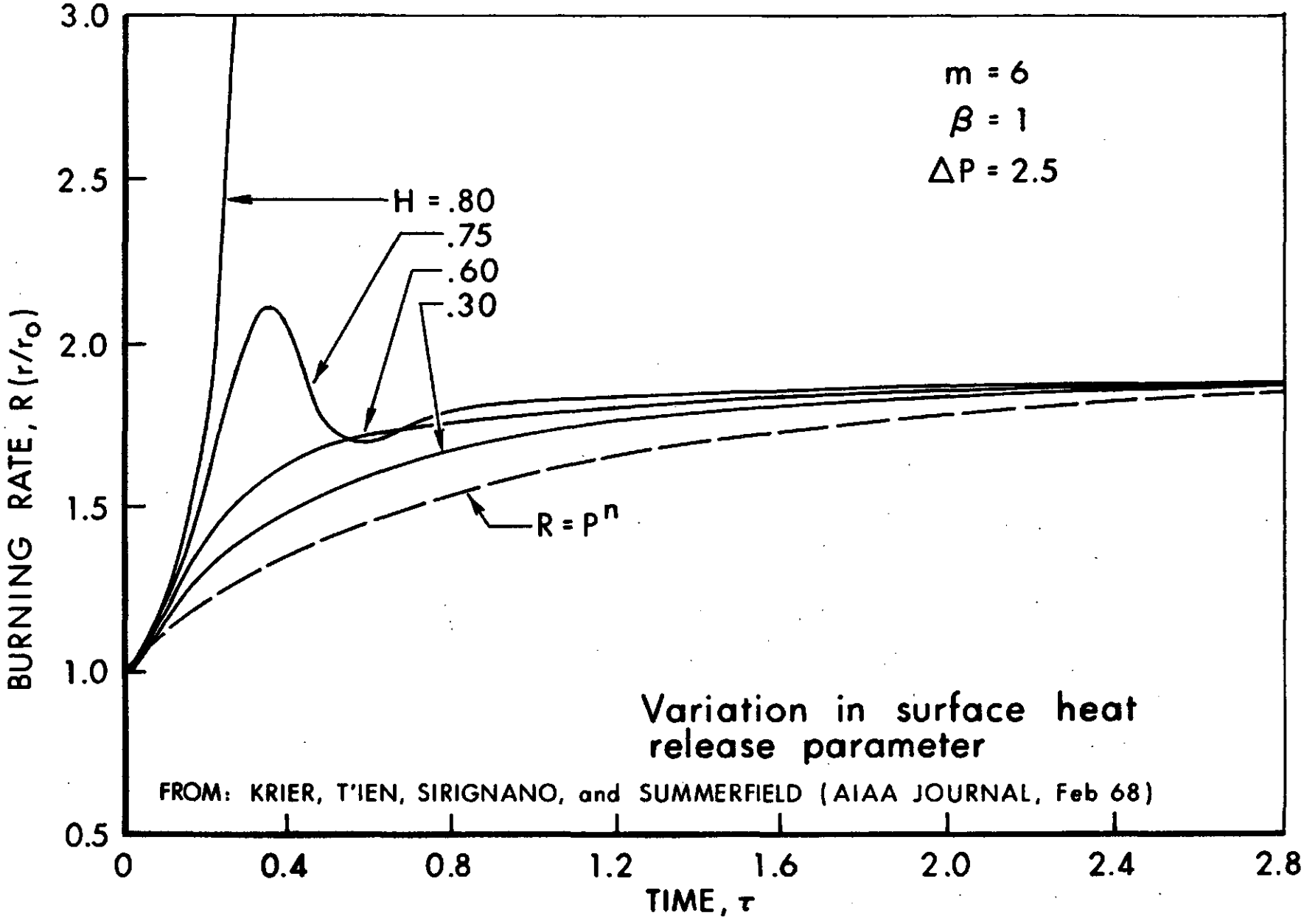

Figure 5. Burning Rate Response of KTSS Model (Original Results)

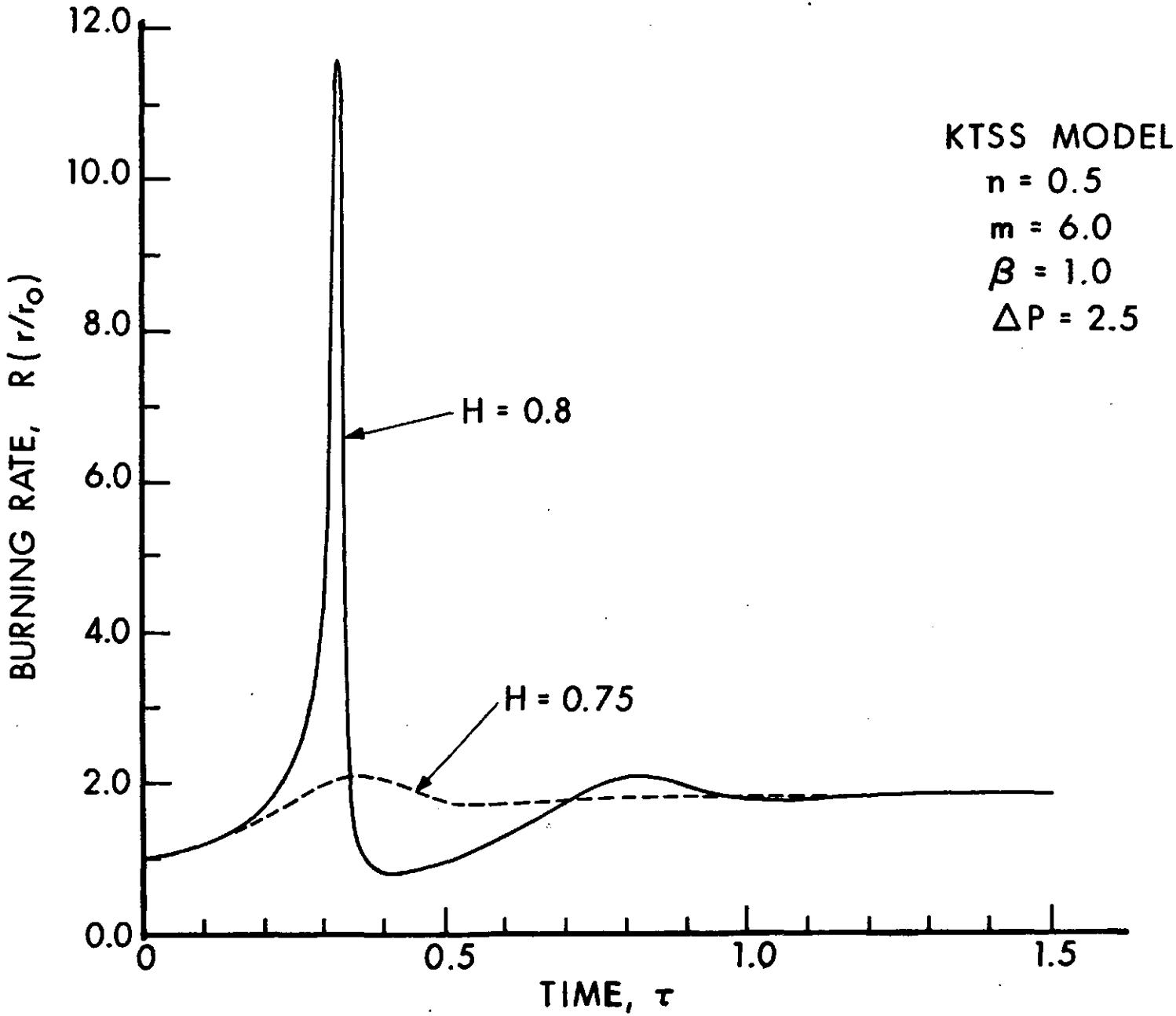

Figure 6. Burning Rate Response of KTSS Model (Recomputed Results)

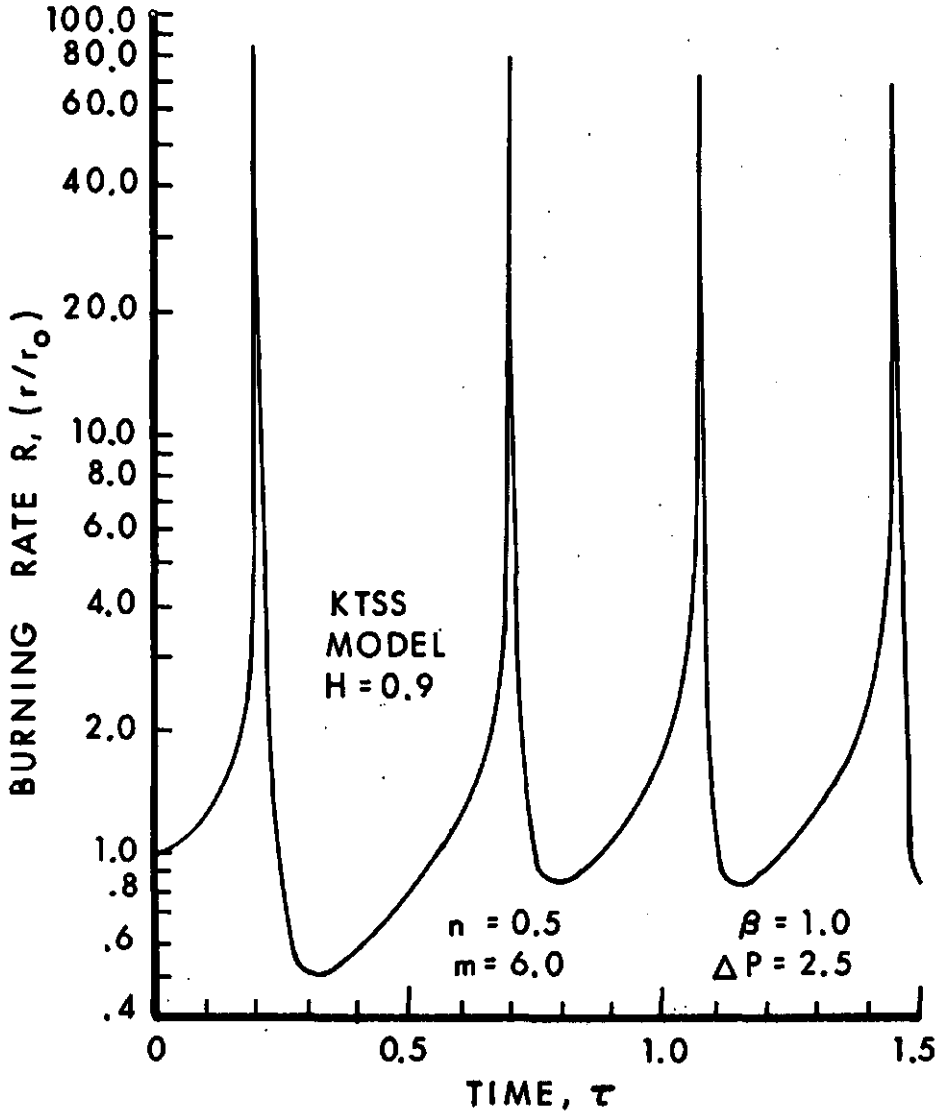

Figure 7. Burning Rate Response of KTSS Model With H=0.9

not consider regression of a gas/solid interface, the burning rate quoted in Ref. 11 is the velocity of the reaction front maximum as it moves into the unreacted solid. For certain values of heat release, the velocity of the reaction front pulsates (see Fig. 5 in Ref. 11) in a manner similar to the present results for surface regression shown in Figs. 7 and 8.

It is also of interest to compare the predictions of all three combustion models under identical input conditions when driven by the same exponential pressure profile [Eq. (28)]. Figure 9 shows the results (Method D) of such a comparison when H = 0.8, n = 0.67, and the remaining parameters are those of Table I.

Table I. Assumed Propellant Parameters

$\rho_s = 1.54$ gm/cm^3

$c_s = 1.55$ J/gm-°K [0.37 cal/gm-°K]

$k_s = 0.0031$ J/cm-sec-°K [7.3×10^{-4} cal/cm-sec-°K]

$\Rightarrow \alpha = 1.28 \times 10^{-3}$ cm^2/sec

$T_\infty = 298$°K

$E_s = 0.0628$ MJ/mole [15 kcal/mole] (m = 6.2, KTSS)

$c_p = 1.72$ J/gm-°K [0.41 cal/gm-°K]

$k_g = 0.00156$ J/cm-sec-°K [3.72×10^{-4} cal/cm-sec-°K]

$r_o = 0.75$ cm/sec

$p_o = 6.9$ MPa [1000 psia] } steady state initial conditions

$T_{so} = 623$°K

Qualitatively, the burning rate response of each model is the same. The large value of peak burning rate predicted by the KTSS model can be traced to the assumption that $c_p = c_s$, which removes the damping term, $R(\Theta_s - 1)(1 - c_p/c_s)$, from the gradient boundary condition. Since it could easily be replaced in the model, this is considered a minor point in the present investigation.

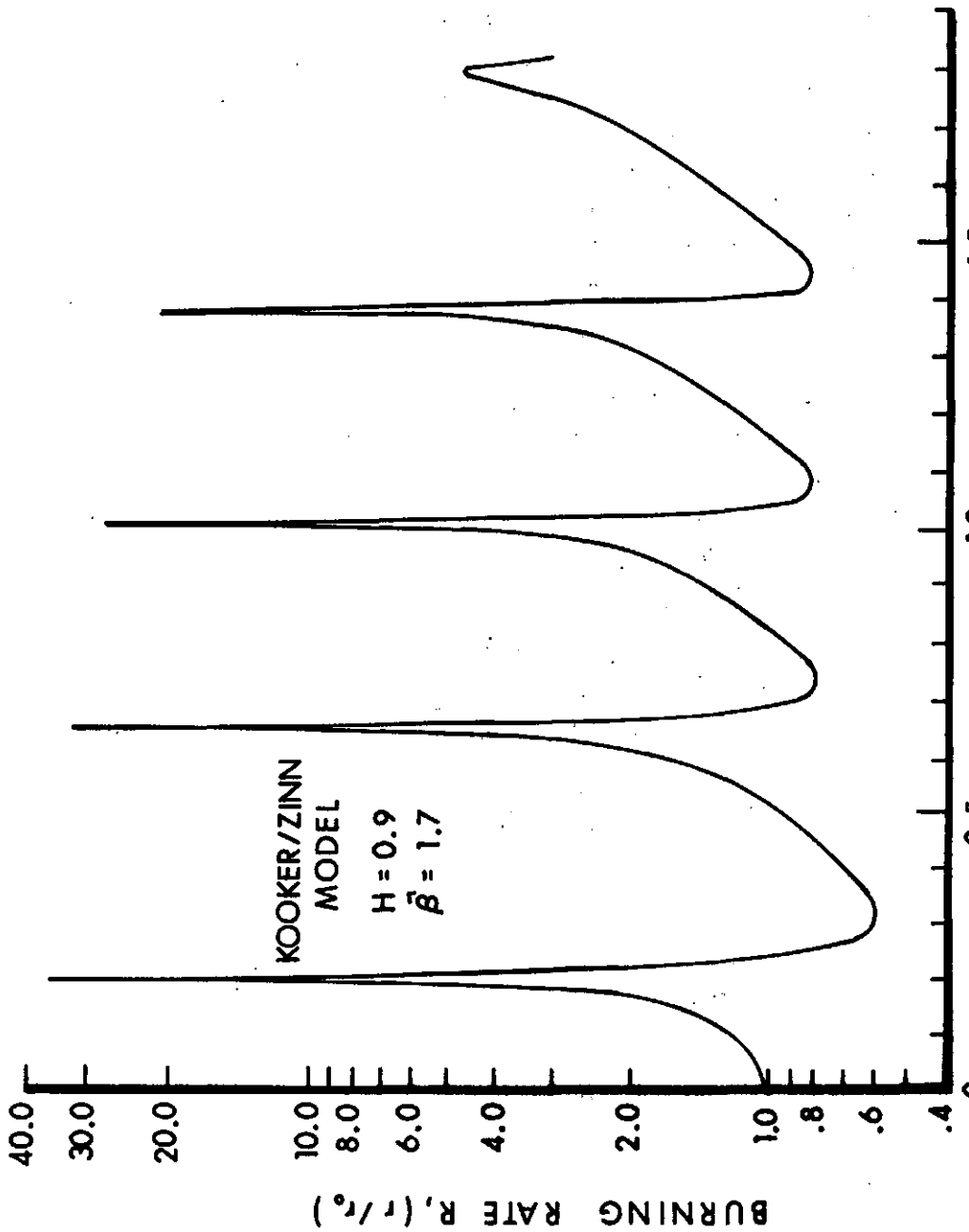

Figure 8. Burning Rate Response of Kooker/Zinn Model with H=0.9, $\hat{\beta}$=1.7

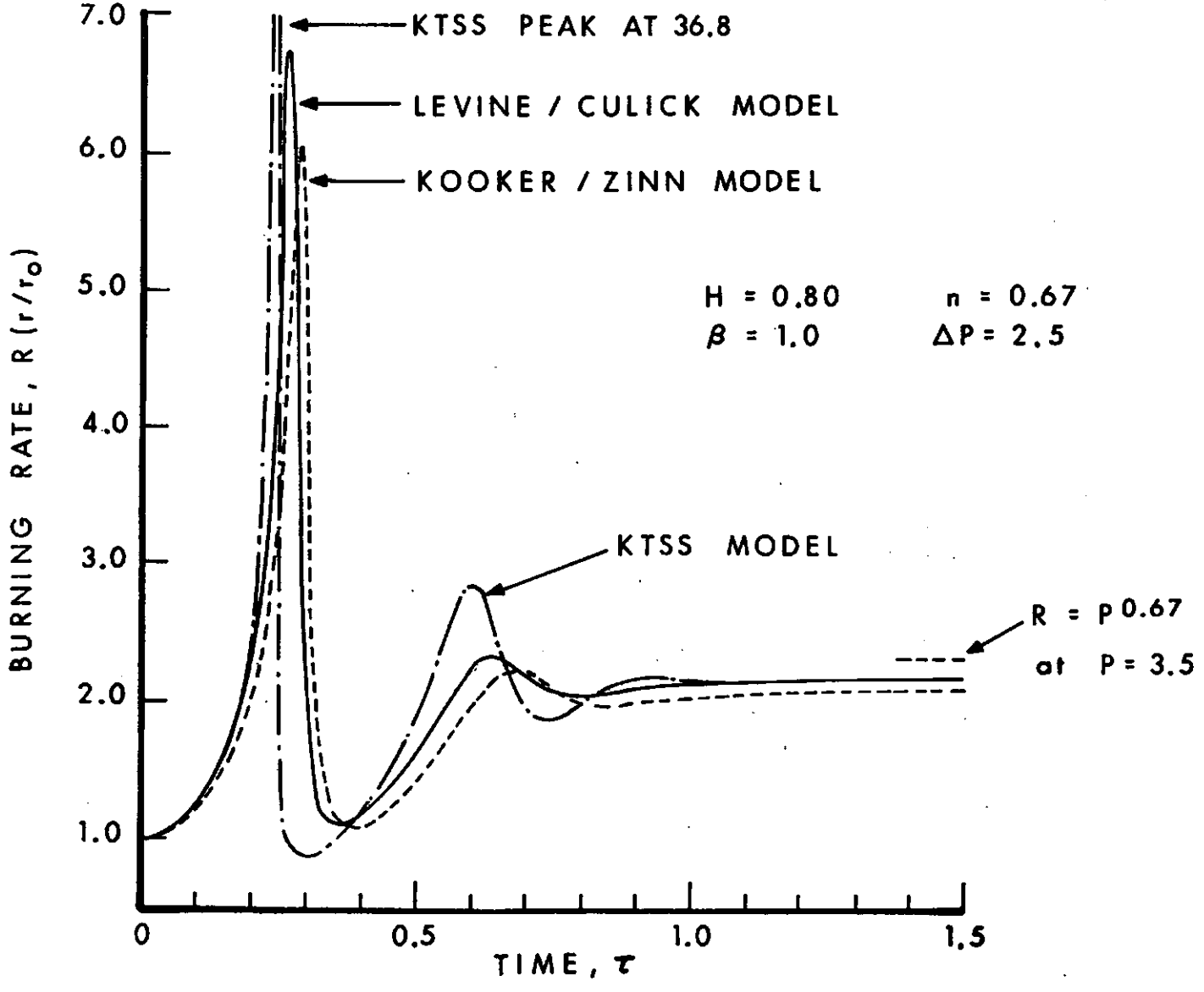

Figure 9. Comparison of Model Predictions for Burning Rate Response to KTSS Pressure Profile

Two important observations can be made from the results displayed in Figs. 6-9. First, the interval of time equal to α/r_o^2 ($\Delta\tau$=1, non-dimensionally), often quoted in theoretical analyses as the characteristic response time of the thermal wave in the unburned solid, is of limited value when estimating the time for a significant change in the burning rate. Secondly, the instantaneous propellant burning rate cannot be characterized as a function of $d\ln P/d\tau$. To dramatize the latter point, consider the following expression for instantaneous burning rate derived recently by Krier (Ref. 13) from a perturbation analysis of the KTSS Model. In the notation of the present report,

$$R(\tau) = R_s\left[1 + \Psi(P)\frac{n}{R_s^2}\frac{d\ln P}{d\tau}\right] \tag{29}$$

where $$\Psi(P) = \frac{\left(1 - \frac{1}{m}P^{n/m}\right)}{\left[P^{n/m}\left(2+\frac{1}{m}\right) - 2H\right]}$$

and $P = P(\tau)$.

Using $R_s = P^n$ and $P(\tau)$ given by the exponential profile in Eq. (28), the numerical predictions of Eq. (29) are compared in Fig. 10 to the full numerical solution (Method D) of the KTSS combustion model for the same set of parameters. Certainly for this example, no correlation exists between the two results in the time interval 0 - 1.0.

B. Burning Rate Response in a Simulated Gun Combustion Chamber

A typical gun propellant is assumed to be represented by the parameters given in Table 1. Also required is a value for the surface heat release (H) associated with the global pyrolysis reaction. This is possibly the most difficult parameter to estimate since a single reaction which converts solid to gas does not exist in the actual combustion process. The present investigation will rely on experimental studies such as Ref. 14 in which estimates are made of the amount of heat released in the surface zone of a double-base propellant, with and without catalysts, under steady state conditions. The results of Ref. 14 are reproduced here as Fig. 11 which indicates that a value

---

[13] *Krier, H., "Solid Propellant Burning Rate During a Pressure Transient," Comb. & Flame, Vol. 5, pp. 69-73 (1972).*

[14] *Kubota, N., Ohlemiller, T. J., Caveny, L. H., and Summerfield, M., "An Experimental Study of the Site and Mode of Action of Platonizers in Double Base Propellants," AIAA Paper 74-124, presented at 12th Aerospace Sciences Meeting (January 1974).*

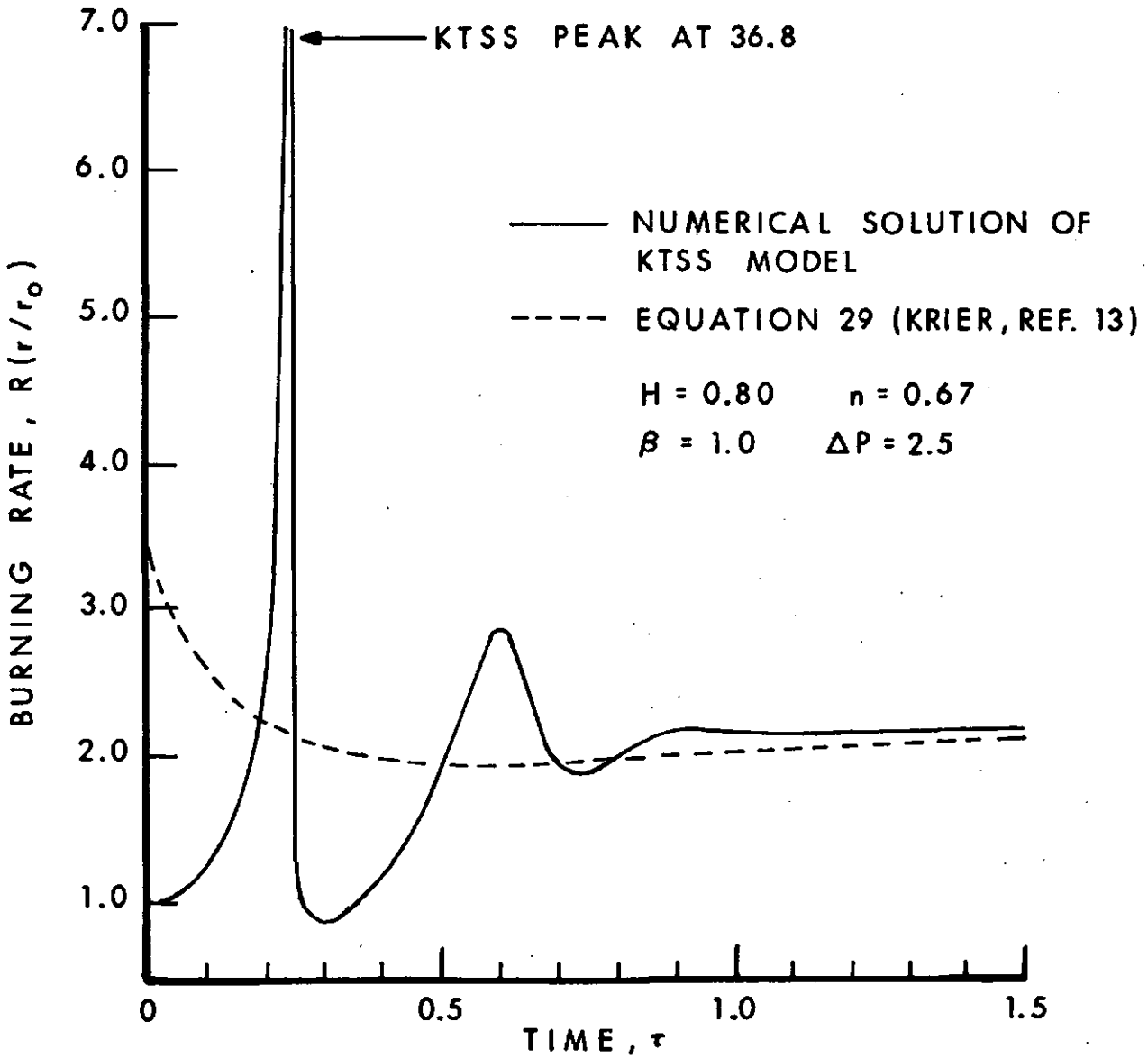

Figure 10. Comparison of Equation 29 with the Numerical Solution (Method D) of the KTSS Model

of approximately 418 J/gm (100 cal/gm) would be compatible with the assumed initial conditions of Table 1. This implies a range of values for H between 0.8 and 0.9. Other investigators (Refs. 15-17) have inferred values of H from 0.5 to 0.85 for double-base propellants.

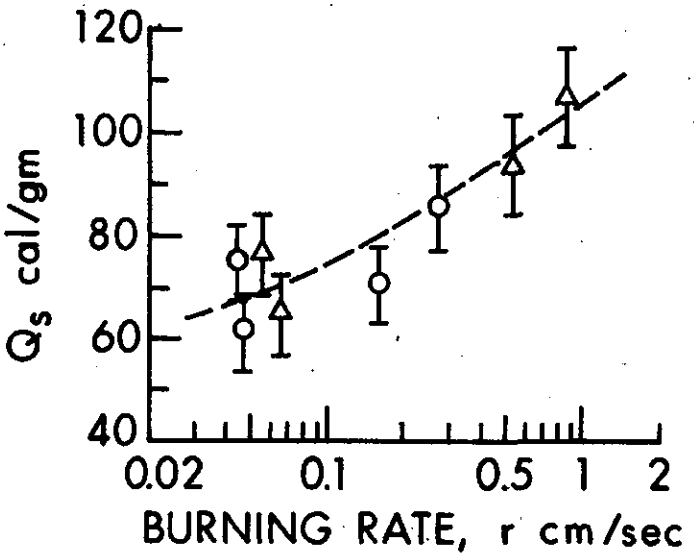

Figure 11. Surface Heat Release vs Burning Rate (Ref. 14)

The pressure variation to be imposed at the edge of the flame zone in the combustion models is obtained from an experimental firing of the 105mm Tank Gun M68 and is illustrated in Fig. 12. The record from this mid-chamber gauge indicates an ignition and flame-spreading delay of about 14 ms. For the purpose of the numerical solution, a time origin (τ=0) is established at the point where the gun pressure is equal to 6.9MPa (1000 psi). From this origin, approximately 1.3 nondimensional time units (~3ms) are required to reach the peak pressure of 393 MPa (57,000 psi).

An example of the burning rate response to the above-mentioned gun pressure-time history is shown in Figs. 13 and 14 for the Levine/

---

[15] *Zenin, A. A., "Structure of Temperature Distribution in Steady State Burning of a Ballistite Powder," Fizika Goreniya i Vzryva, Vol. 2, No. 3, pp. 67-76 (1966).*

[16] *Koval'skii, A. A., Konev, E. V., and Krasil'nikov, B. V., "Combustion of Nitroglycerine Powder," Fizika Goreniya i Vzryva, Vol. 3, No. 4, pp. 547-554 (1967).*

[17] *Ibiricu, M. M., and Williams, F. A., "Mechanisms for the Steady Deflagration of Double Base Propellants," 12th JANNAF Combustion Meeting, Newport, RI, CPIA Publication 273 (1975).*

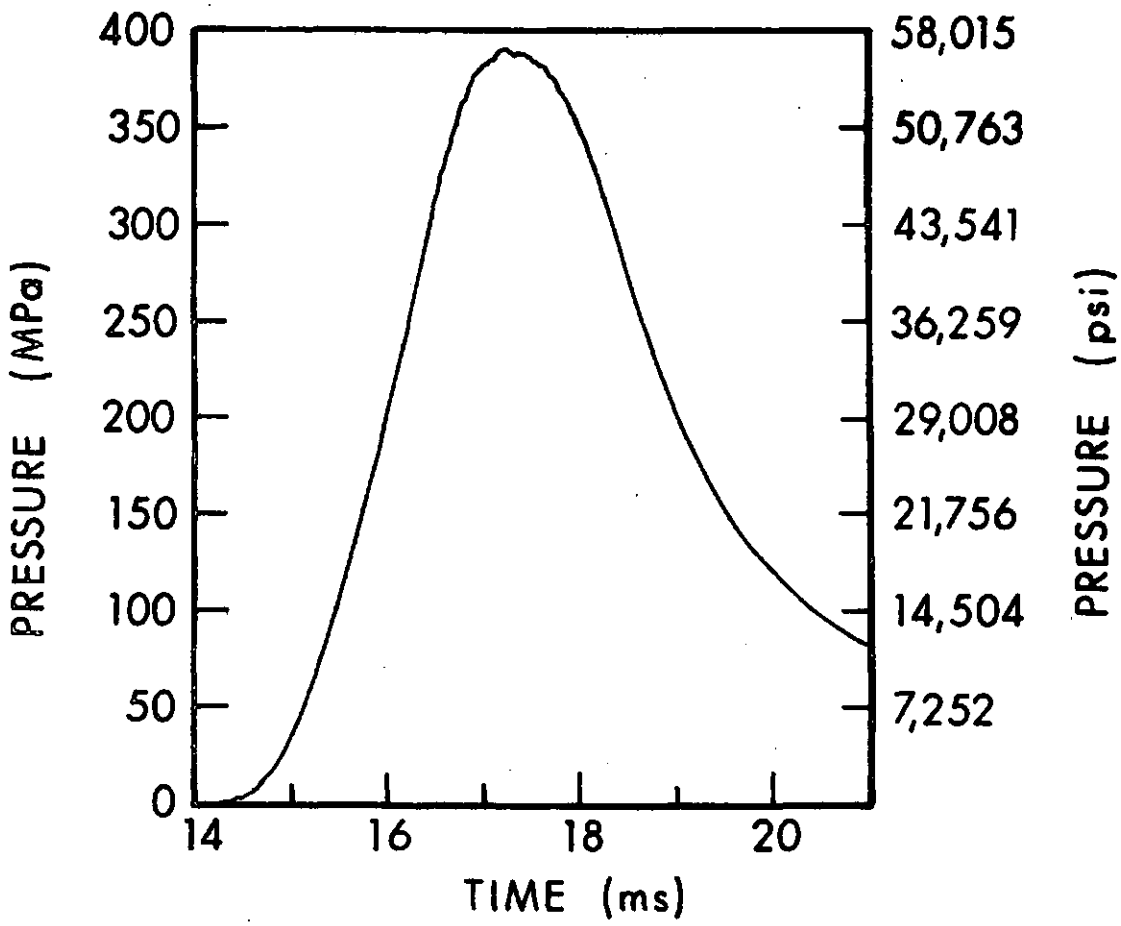

Figure 12. 105mm Gun Pressure Time-History

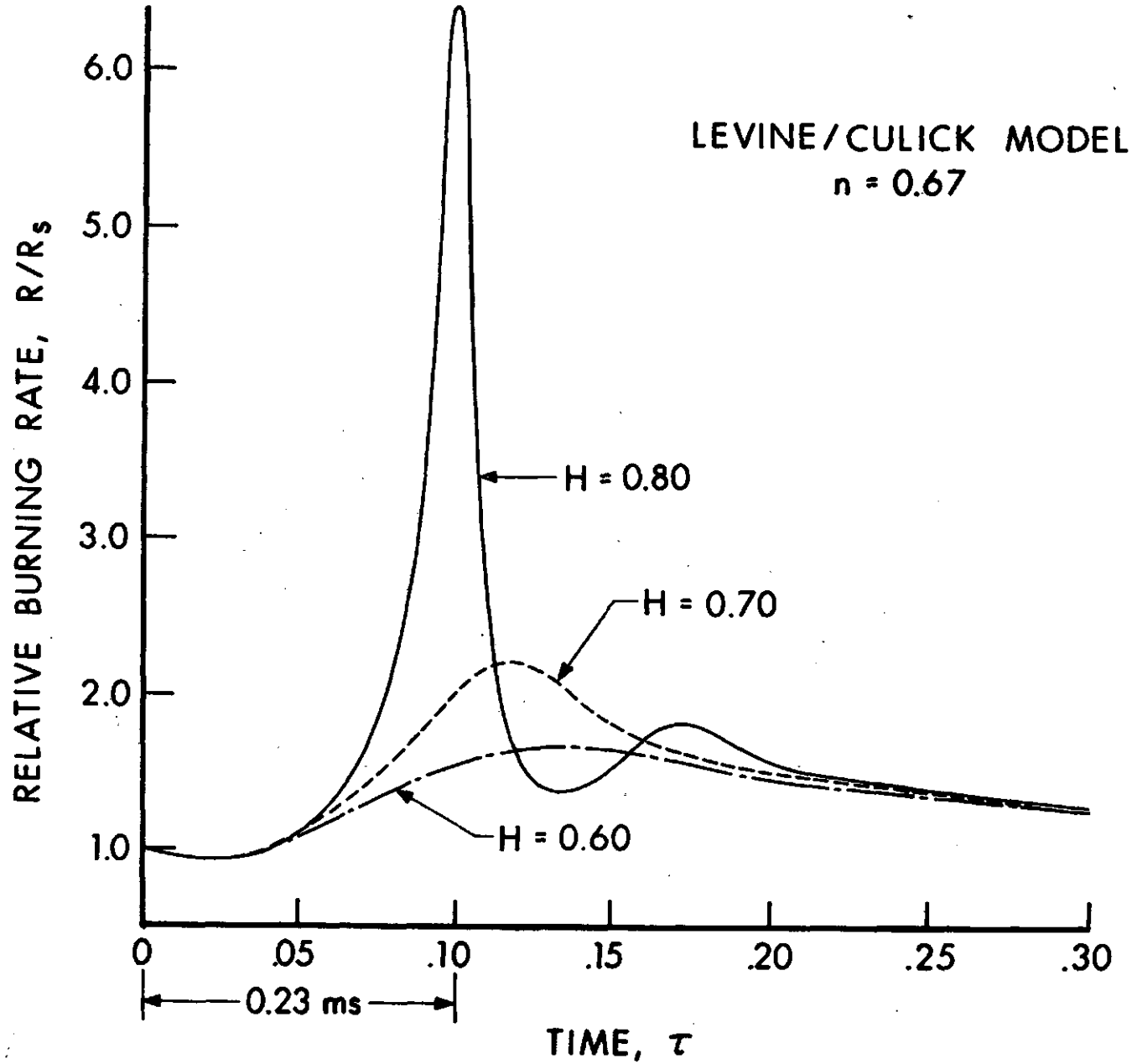

Figure 13. Influence of a Change in Surface Heat Release on Burning Rate Response to Gun Pressure Time-History

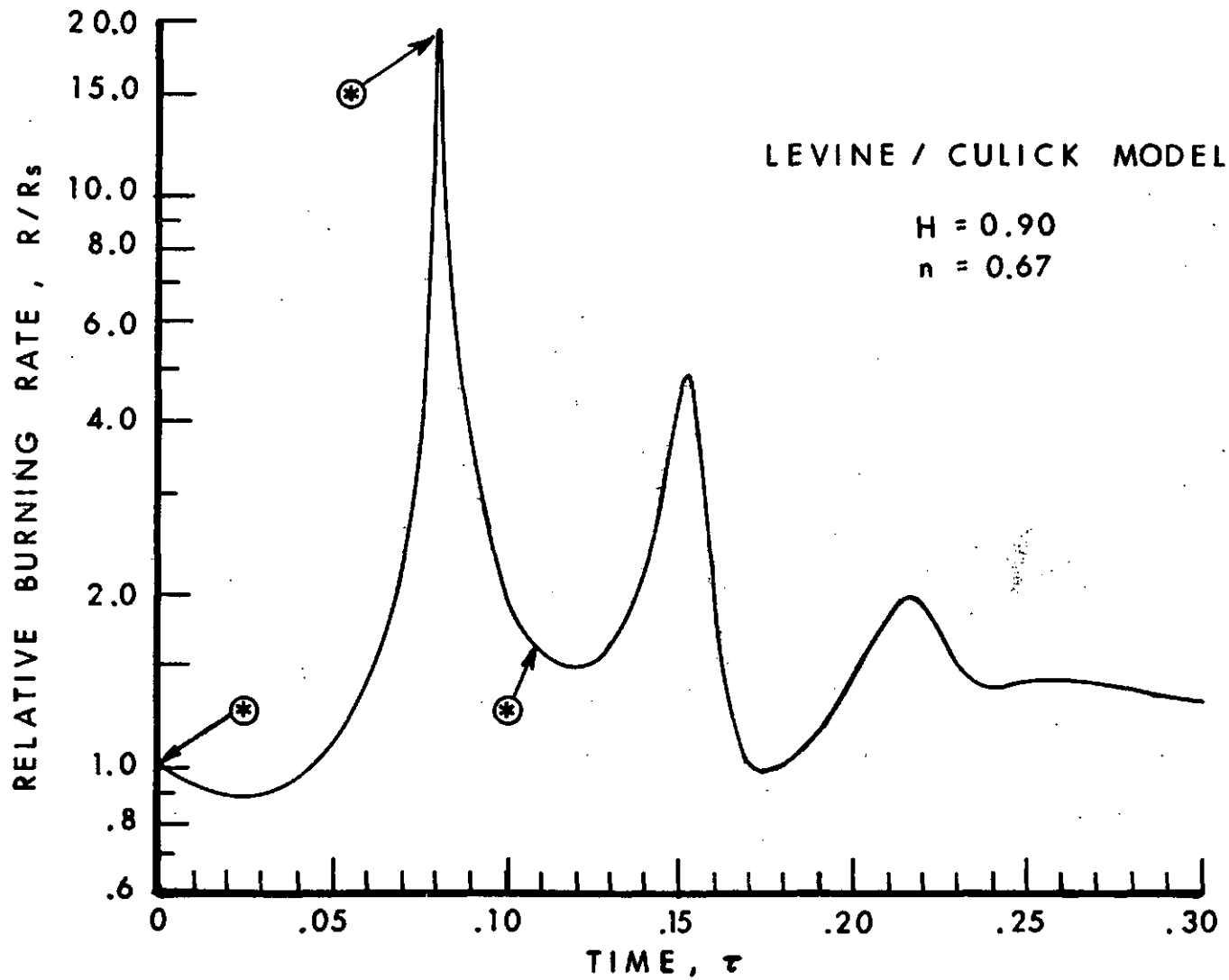

Figure 14. Burning Rate Response to Gun Pressure Time-History

Culick model using Method D. The results are plotted as R/R_S, where R_S is the steady state value of burning rate based on the instantaneous value of pressure and the pressure exponent, n = 0.67. Note that, at first, R/R_S falls below one, indicating that the thermal wave which controls burning rate does not respond instantaneously to the increasing pressure. The figures clearly show the sensitivity of the combustion model as H increases. For a value of H = 0.9, the numerical solution indicates a maximum dynamic overshoot of approximately 20. To see if this behavior follows from unrealistic variations of the temperature distribution in the solid propellant, the thermal profile for three points in time (as denoted by the symbols in Fig. 14) is plotted in Fig. 15. The curve for $\tau = 0$ is the initial thermal wave at steady state which decays to 1/e of the surface value in a distance of α/r_o (or $\eta = 1$). When the burning rate is maximum, the distribution shows a surface temperature of 880°K and a very steep gradient in the region close to the interface. This is the result of a heating rate at $\eta = 0^+$ (surface reaction plus flame reaction) which has been greater than the rate at which heat can be conducted into the unburned solid without raising the surface temperature. At the maximum burning rate, this imbalance reverses. The burning rate then declines as a result of the combined effects of (1) rapid heat conduction into the unburned solid due to the steep thermal profile near the surface, and (2) the large regression rate which is continuously moving lower temperature propellant closer to the surface. In this example as well as those shown in Figs. 7 and 8, the declining burning rate is accelerated by the exponential dependence of the surface heat release term on propellant surface temperature (i.e., the RH term). The profile at $\tau = 0.106$ shows that the maximum thermal gradient is located in the interior region. At this lower value of burning rate, the gradient at the surface is much less than its previous maximum at $\tau = 0.080$, and hence the surface heat conduction rate is much lower. However, the rate of heat release in the flame zone continues to increase with the increasing pressure. Thus, a new dynamic cycle begins. The multiple spike pattern in Figs. 7 and 8 is created in the same way.

The influence of the numerical method of integration (Methods B, C, D) on the final burning rate prediction is examined in Fig. 16 using the Levine/Culick combustion model with H = 0.80 and n = 0.67 as an example. The results show a close agreement except near the peak burning rate. In the vicinity of the peak, Method D predicts a larger value than Methods (B) and (C) which are coincident. After considerable study, it was determined that the difference is attributable to errors in the matrix inversion process used by both Methods (B) and (C). For these implicit solutions where the time step is much larger than the explicit diffusion stability limit, a loss of diagonal dominance can occur when the regression rate R is large (see Eqs. 26 and 27). In a special exercise, the time step $\Delta\tau$ and the grid spacing $\Delta\eta_j$ near the propellant

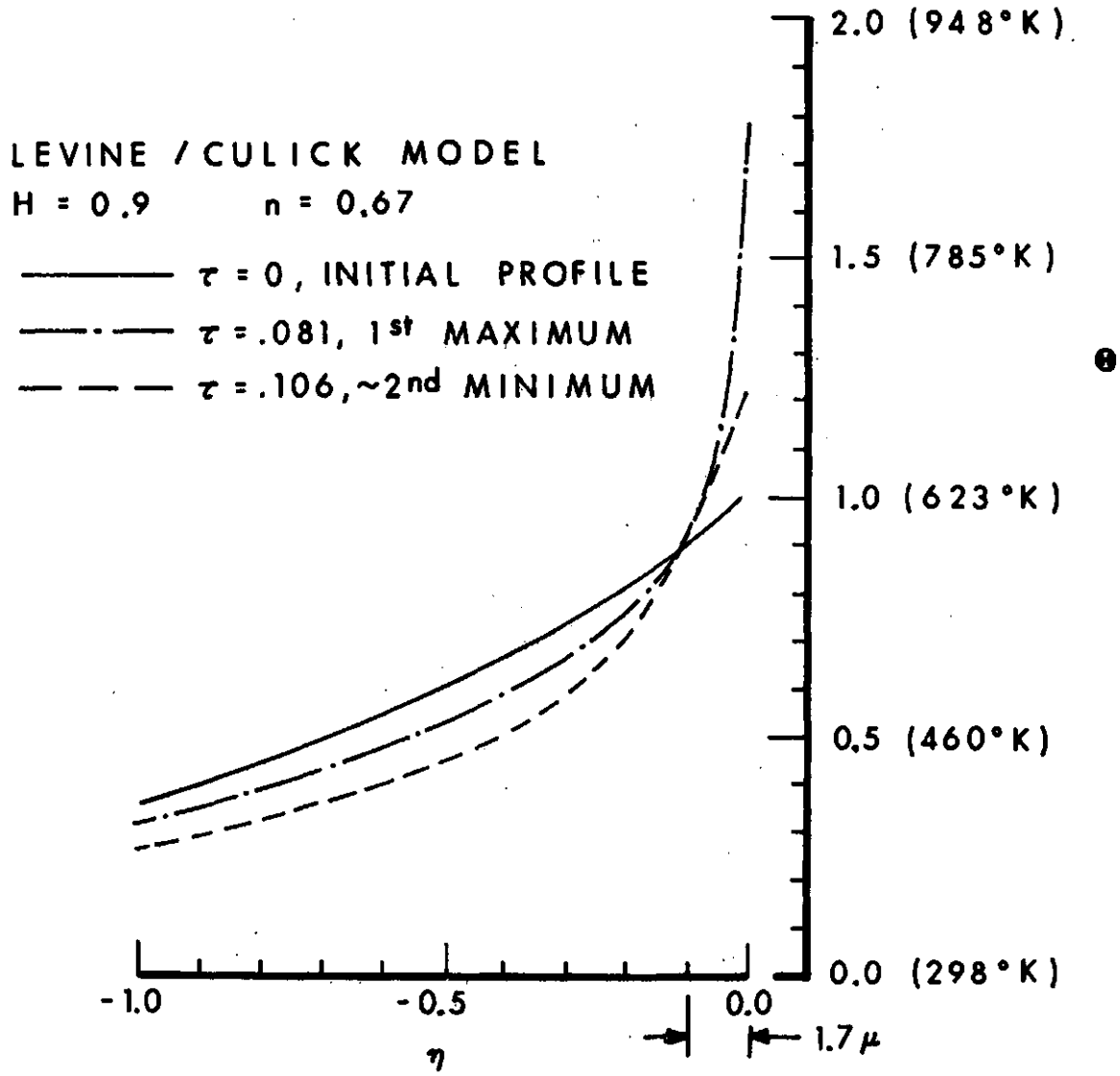

Figure 15. Temperature Profiles in Unburned Solid Propellant

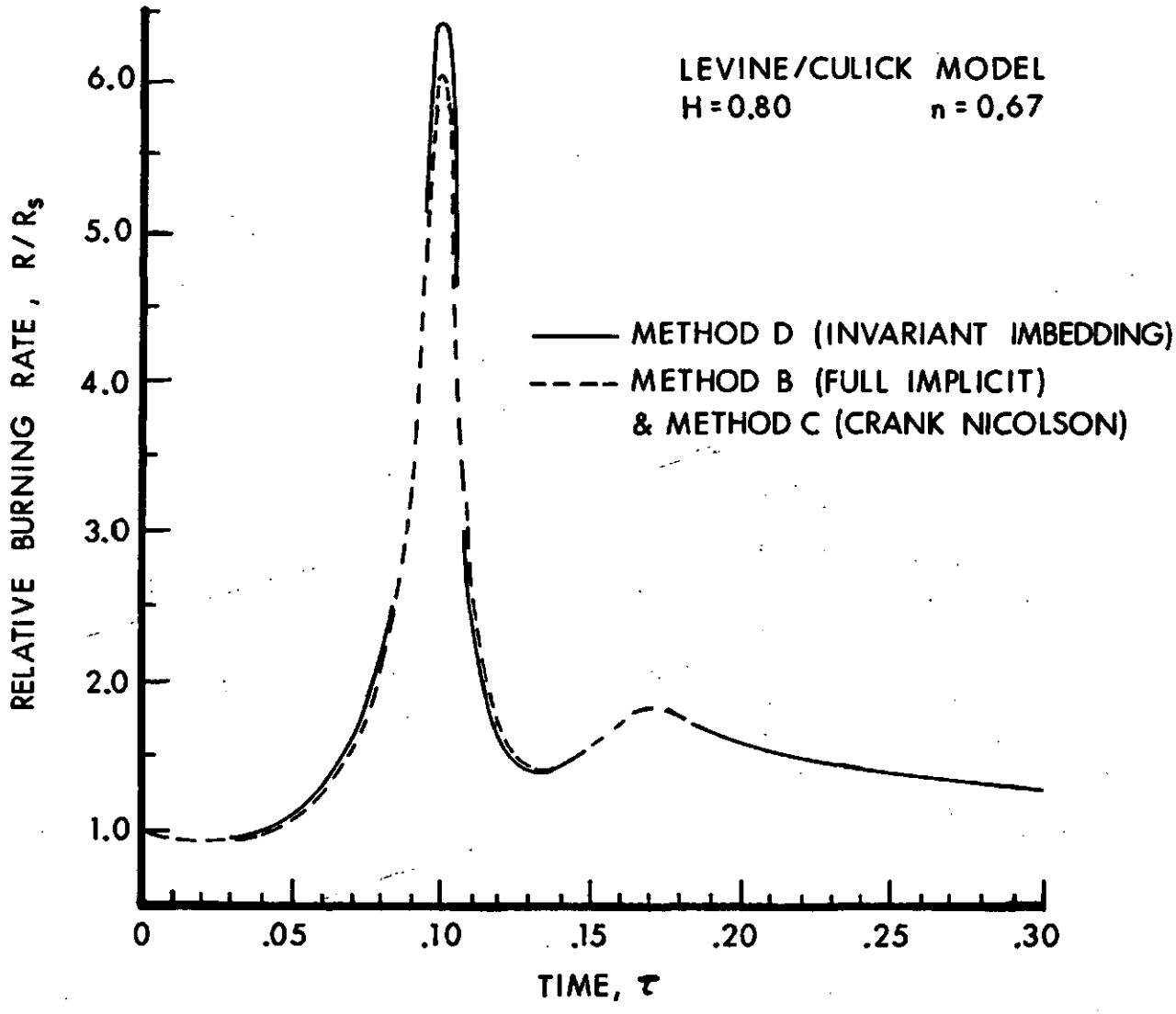

Figure 16. Comparison of Burning Rate Response Predicted by Three Numerical Integration Methods

interface were manipulated to maintain diagonal dominance as the regression rate became large; the numerical result for peak burning rate then matched the Method (D) result to within a fraction of a percent. This verifies the hypothesis but the required manipulation is uneconomical. It should be emphasized that, at all times, the numerical solutions obtained with Methods (B) and (C) were stable and smooth. Prof. Gino Moretti's well-known statement about the dangers of "confusing smoothness with accuracy" is definitely applicable here. For reasons beyond the scope of this report, Method (D) (invariant imbedding) is not subject to the diagonal dominance limitation and is considered the superior method, in both accuracy and economy.

The influence of a change in the steady state pressure exponent n is demonstrated in Fig. 17 with the Levine/Culick model, again using Method D. The larger value of n leads to approximately the same relative burning rate response, but at an earlier time. The response of all three combustion models to the gun pressure-time history is shown in Fig. 18 using the larger value of n. Again the predictions are qualitatively the same; in all the models, the dynamic burning rate is ultimately controlled by the response of the thermal wave in the unburned solid.

C. Burning Rate Response in a Simulated Closed Bomb

A simple problem was devised to estimate the effect of dynamic burning rate on closed-bomb measurements. The propellant is assumed to be burning at steady state until $\tau = 0$ when it is suddenly confined. The imposed pressure is then given by

$$P(\tau) = 1.0 + \int_0^{\tau} R d\hat{\tau} \quad . \tag{30}$$

The numerical predictions (Method D) following from the Levine/Culick model (with the same parameter values as in Fig. 18) and the steady state "model" $R = P^n$ are compared in Fig. 19. A dynamic overshoot of approximately 3 occurs at low pressure (early time) but the visible effect disappears rapidly thereafter. If the results below 35 MPa (5 kpsi) were discarded when analyzing this simulated closed-bomb experiment, the dynamic effects would go undetected.

CONCLUSIONS

1. "Intrinsic burning rate instability" (or runaway) is a numerical difficulty and is not a solution to the thermal-wave combustion models. The nonlinear models admit large-amplitude, sharp "spikes" in burning rate as a response to a monotonically increasing pressure field, but the numerical solutions remain finite.

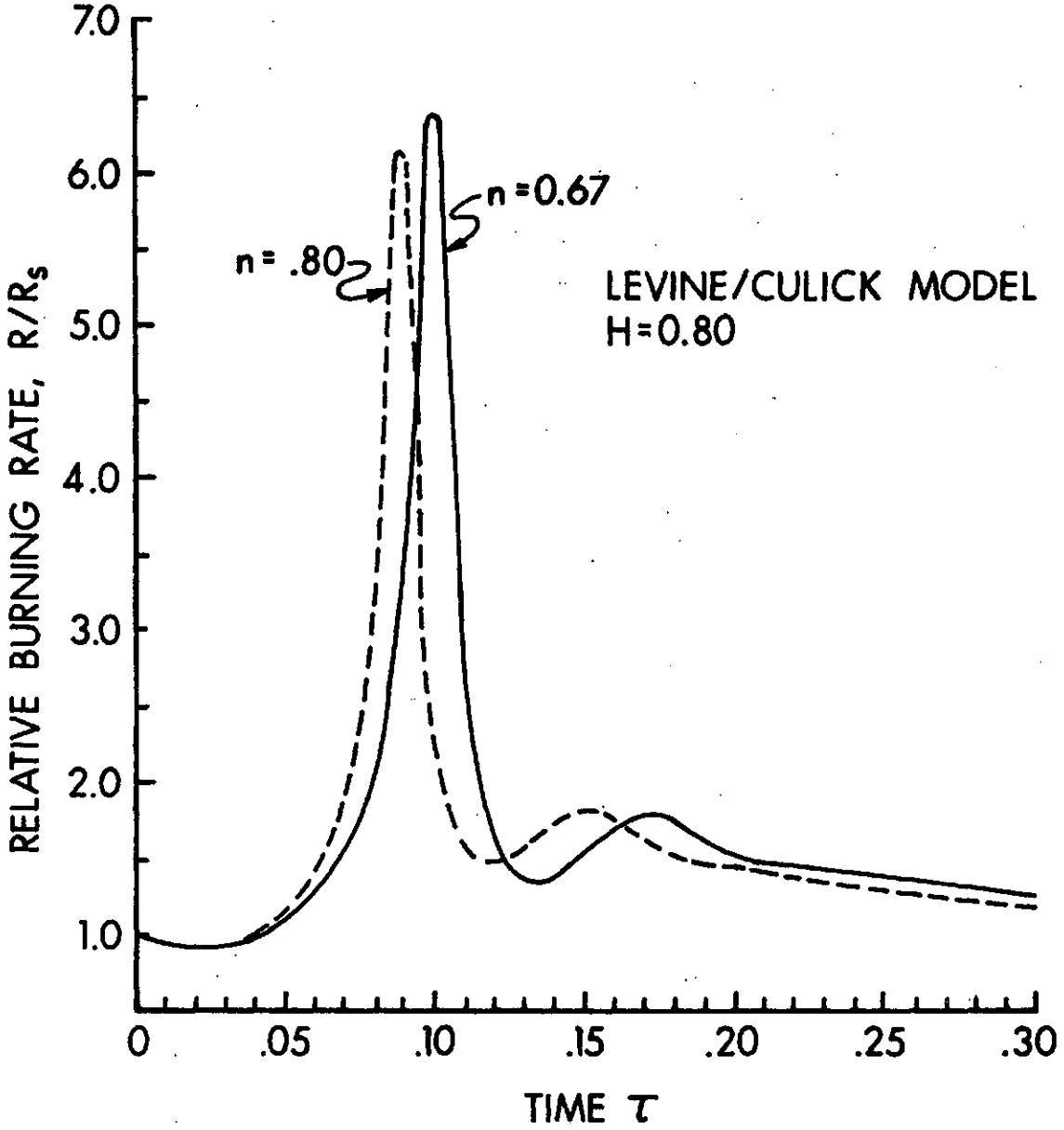

Figure 17. Influence of a Change in Pressure Index "n" on Burning Rate Response to Gun Pressure Time-History

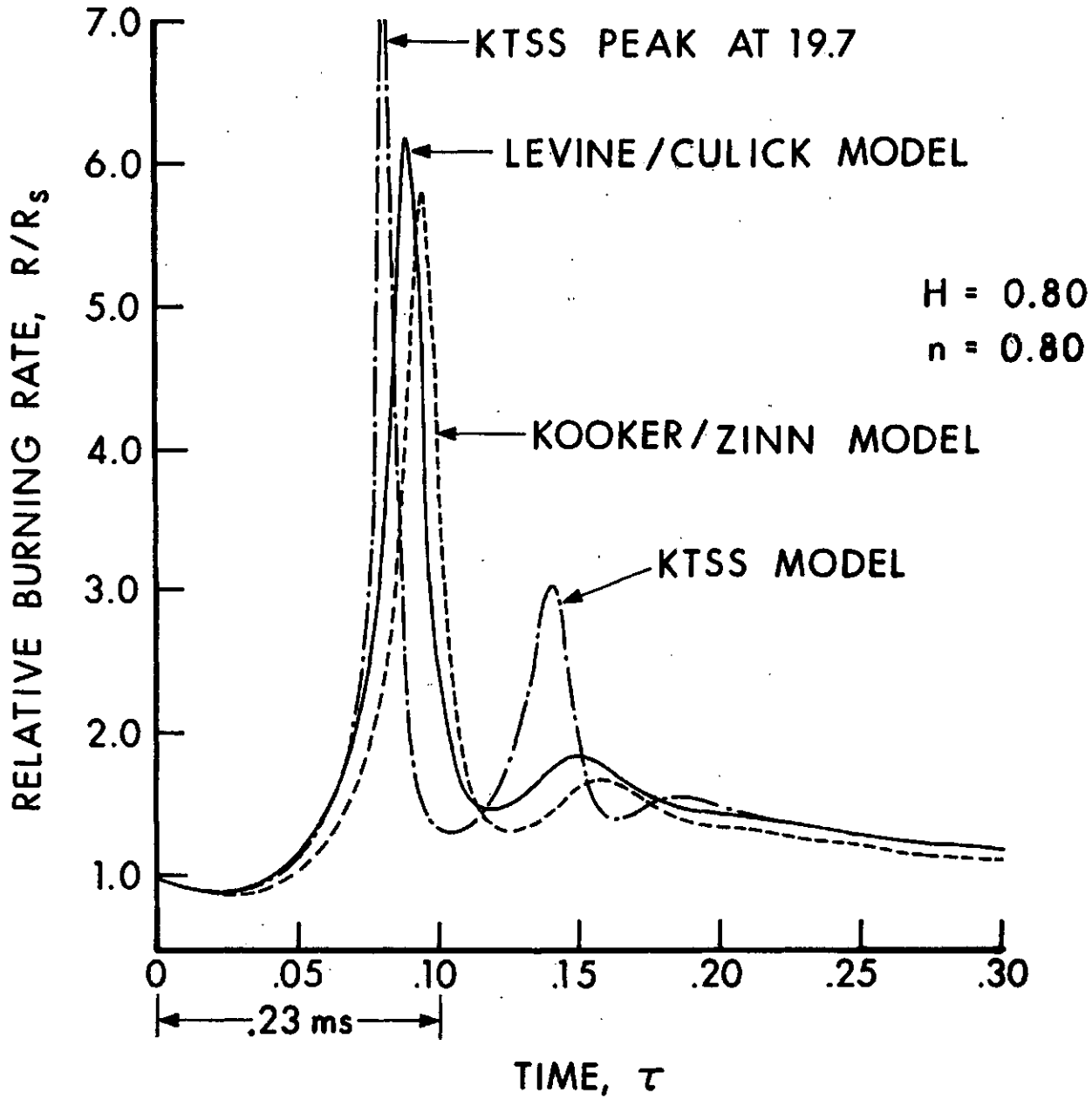

Figure 18. Comparison of Model Predictions for Burning Rate Response to Gun Pressure Time-History

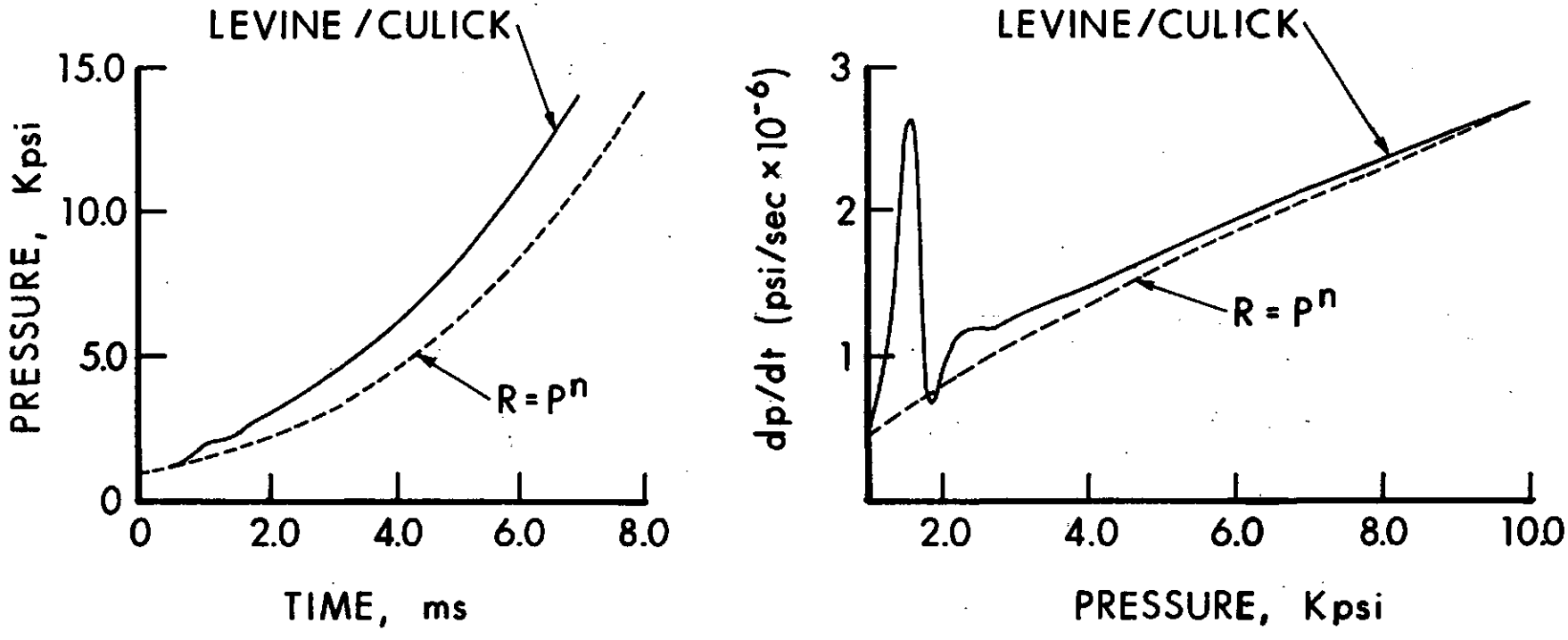

Figure 19. Simulated Closed-Bomb Results Using the Levine/Culick Model with H=0.8, n=0.8

2. When the combustion models are driven by a gun pressure-time history or a simulated closed-bomb environment, the combustion response at low pressure (early time) can be much greater than the "steady state" prediction provided by ap^n, while the response at high pressure returns asymptotically to ap^n. For the closed-bomb problem considered here, the dynamic response of the propellant would go undetected if the pressure record below 35 MPa (5 kpsi) were discarded.

3. Given the major assumption of a quasi-steady flame region, all three combustion models predict nearly the same burning rate response regardless of the differences in the analysis of the gas-phase flame zone. For these models, the dominant influence is the response of the thermal wave in the unburned solid.

4. The interval of time equal to α/r_o^2, often quoted in theoretical analyses as the characteristic response time of the solid propellant, can be misleading when used to estimate the time for a significant change in the burning rate. The present results show that substantial changes in burning rate can occur in a time interval which is an order of magnitude smaller than the characteristic response time.

5. Simplified expressions for instantaneous propellant burning rate, derived from a given combustion model using linearized analysis (such as Ref. 13), can yield erroneous trends when compared to the numerical solution of the complete model.

6. Based on the three combustion models investigated here, the dynamic burning rate is very sensitive to the amount of heat released in the surface reaction. Future modeling efforts should concentrate on a detailed description of the physical and chemical changes which occur at or near the propellant surface.

Important Implication of Conclusions

The present investigation has demonstrated that three thermal-wave solid propellant combustion models, based on the assumption of a quasi-steady flame zone, predict the possibility of rapid, large-amplitude dynamic burning rate excursions from the steady state law, ap^n. Except for the simulated closed-bomb example, these calculations have assumed that the pressure variations and the propellant burning rate are uncoupled, i.e. the pressure field is simply imposed at the edge of the flame zone. Of course, in the actual gun combustion chamber, these two phenomena are coupled. In close analogy to the combustion instability problem in a rocket engine, the pressure disturbance and the dynamic burning rate response it creates could be "in-phase" with each other, where one will reinforce the other. The study of rocket instability in Ref. 9 found that under in-phase con-

ditions a dynamic burning rate response of 3-4 would sustain a longitudinal pressure disturbance in the rocket engine; it should be noted here that the continuous outflow through the nozzle represents a substantial loss mechanism to the disturbance flow field in the chamber. If the sum of the loss mechanisms inherent in the gun combustion chamber flow field are the same order of magnitude as a rocket nozzle, then a similar behavior would be expected. Hence, once a pressure disturbance is created in a gun system, the dynamic burning rate could easily be responsible for driving and sustaining a large amplitude pressure wave in the combustion chamber.

APPENDIX

Application of Invariant Imbedding

Following Ref. A1, Invariant Imbedding [Method (D)] is applied to a second-order linear partial differential equation in the following manner. Consider the system (for an arbitrary dependent variable, u)

$$u_t + Ru_x - u_{xx} = 0 \quad [-x_o \le x \le 0] \tag{A1}$$

initial condition

$$u(x,0) = u_o(x) \tag{a}$$

boundary conditions

$$u(-x_o,t) = 0 \tag{b}$$

$$u_x(0,t) = G(u,t). \tag{c}$$

Using the method-of-lines, let

$$u_t \cong (u - u^{n-1})/\Delta t. \tag{A2}$$

Also define,

$$\psi \equiv du/dx = u'. \tag{A3}$$

Then Eq. (A1) can be written as the equivalent first-order system given by

$$u' = \psi \,, \tag{A4}$$

$$\psi' = R\psi + \frac{1}{\Delta t}(u - u^{n-1}) \,. \tag{A5}$$

If Eqs. (A4) and (A5) are viewed as characteristic equations for an initial value problem, then characteristic theory states that the solution of Eqs. (A4) and (A5) generates the integral surface $u(x,\psi)$ of the equation

$$u_x + u_\psi \left[R\psi + \frac{1}{\Delta t}(u - u^{n-1})\right] = \psi \,. \tag{A6}$$

The general solution to Eq. (A6) has been shown by Meyer (Ref. 18) to be

$$u(x,\psi) = V(x)\psi + W(x) \,. \tag{A7}$$

A1 *Meyer, G. H., Initial Value Methods for Boundary Value Problems (Theory and Application of Invariant Imbedding), 100th Volume in the Series Mathematics in Science and Engineering, ed. R. Bellman, Academic Press, NY (1973).*

Substituting Eq. (A7) into Eq. (A6) yields an equation for both V and W,

$$V' = 1 - RV - V^2/\Delta t \ , \tag{A8}$$

$$W' = -V(W - u^{n-1})/\Delta t \ . \tag{A9}$$

The initial conditions required for these two equations follow from a compliance with the boundary condition (A1b) at $-x_o$,

$$V(-x_o) = 0, \quad W(-x_o) = 0 \ . \tag{A10}$$

Substitution of Eq. (A7) into Eq. (A5) gives the equation governing ψ,

$$\psi' = (R + V/\Delta t)\psi + (W - u^{n-1})/\Delta t \ . \tag{A11}$$

The initial value of ψ follows directly from the gradient boundary condition (A1c) at x=0, i.e.

$$\psi(0) = G\Big|_{\text{new time level.}} \tag{A12}$$

The sequence of computation is then the following:

1. Integrate Eqs. (A8) and (A9) from $-x_o$ to 0 based on the initial values given by Eq. (A10).

2. Satisfy Eq. (A12) at the boundary x=0.

3. Since V(x) and W(x) are now known, integrate Eq. (A11) for $\psi(x)$ from 0 to $-x_o$.

4. Evaluate u(x) at the new time level from Eq. (A7).

It may be noted that Eq. (A8) is a Riccati equation which, along with the initial condition Eq. (A10), has the exact solution,

$$V(x) = [S \coth \zeta + R/2]^{-1} \tag{A13}$$

where $\zeta \equiv S(x + x_o) \quad [-x_o \le x \le 0]$,

and $S \equiv [(R/2)^2 + 1/\Delta t]^{1/2}$.

This eliminates the need to numerically integrate Eq. (A8) in the computation sequence listed above.

Nonlinear Equation

Since the equation and the gradient boundary condition which govern the combustion models are nonlinear, a modification to the above procedure is required. For these models, the coefficient R and the function G are both dependent on u(0) at the new time level. Hence an iteration cycle is created between steps (1) and (2) above; (a) an initial guess or the last iterative value of u(0) is used to integrate Eq. (A8) and estimate the value of G, (b) Eq. (A12) then determines $\psi(0)$, and (c) a new value of u(0) is found from Eq. (A7). The cycle must be repeated until convergence is obtained. The computation then continues to step (3).

This page Left Intentionally Blank

REFERENCES

1. Gough, P. S. and Zwarts, F. J., "Theoretical Model for Ignition of Gun Propellant", Report SRC-R-67, Space Research Corp. (December 1972); also Gough, P. S., "Fundamental Investigation of the Interior Ballistics of Guns", Report SRC-R-74, Space Research Corp. (August 1974).

2. Krier, H., Van Tassell, W., Rajan, S., and VerShaw, J. T., "Model of Gun Propellant Flame Spreading and Combustion", BRL-CR-147 (March 1974), AD #918832L; also Krier, H., "Predictions of Flame-spreading and Pressure Wave Propagation in Propellant Beds", AAE 75-6, University of Illinois (July 1975).

3. Kuo, K., Vichnevetsky, R., and Summerfield, M., "Theory of Flame Front Propagation in Porous Propellant Charges Under Confinement," AIAA Journal, Vol. 11, No. 3, pp 444-451 (April 1973).

4. Fisher, E. B., and Trippe, A. P., "Development of a Basis for Acceptance of Continuously Produced Propellant," Report VQ-5163-D-1, Calspan Corp. (November 1973).

5. East, J. L., and McClure, D. R., "Projectile Motion Predicted by a Solid/Gas Flow Interior Ballistic Model", 10th JANNAF Combustion Meeting, CPIA Publication 243 (August 1973).

6. Baer, P. G., and Frankle, J. M., "The Simulation of Interior Ballistic Performance of Guns by Digital Computer Program," BRL Report 1183 (December 1962), AD #299980.

7. Krier, H., T'ien, J. S., Sirignano, W. A., and Summerfield, M., "Nonsteady Burning Phenomena of Solid Propellants: Theory and Experiments", AIAA Journal, Vol. 6, No. 2, pp 278-285 (February 1968).

8. Levine, J. N., and Culick, F. E. C., "Nonlinear Analysis of Solid Rocket Combustion Instability," AFRPL-TR-74-45 (October 1974).

9. Kooker, D. E., and Zinn, B. T., "Numerical Investigation of Non-linear Axial Instabilities in Solid Rocket Motors," BRL-CR-141 (March 1974), AD #776954, [see also AIAA Paper 73-1298].

10. Carslaw, H. S., and Jaeger, J. C., Conduction of Heat in Solids, Oxford Press, 2nd Edition (1959).

11. Shkadinskii, K. G., Khaikin, B. I., and Merzhanov, A. G., "Propagation of a Pulsating Exothermic Reaction Front in the Condensed Phase," Fizika Goreniya i Vzryva, Vol. 7, No. 1, pp 19-28 (1971).

REFERENCES

12. Bradley, H. H., Jr., "Theory of Ignition of a Reactive Solid by Constant Energy Flux," Comb. Sci. and Tech., Vol. 2, pp 11-20 (1970).

13. Krier, H., "Solid Propellant Burning Rate During a Pressure Transient," Comb. and Flame, Vol. 5, pp 69-73 (1972).

14. Kubota, N., Ohlemiller, T. J., Caveny, L. H., and Summerfield, M., "An Experimental Study of the Site and Mode of Action of Platonizers in Double Base Propellants," AIAA Paper 74-124, presented at 12th Aerosapce Sciences Meeting (January 1974).

15. Zenin, A. A., "Structure of Temperature Distribution in Steady State Burning of a Ballistite Powder," Fizika Goreniya i Vzryva, Vol. 2, No. 3, pp 67-76 (1966).

16. Koval'skii, A. A., Konev, E. V., and Krasil'nikov, B. V., "Combustion of Nitroglycerine Powder," Fizika Goreniya i Vzryva, Vol. 3, No. 4, pp 547-554 (1967).

17. Ibiricu, M. M., and Williams, F. A., "Mechanisms for the Steady Deflagration of Double Base Propellants," 12th JANNAF Combustion Meeting, Newport, RI, CPIA Publication 273 (1975).

A1. Meyer, G. H., Initial Value Methods for Boundary Value Problems (Theory and Application of Invariant Imbedding), 100th Volume in the series Mathematics in Science and Engineering, ed. R. Bellman, Academic Press, NY (1973).

DISTRIBUTION LIST

No. of Copies	Organization
12	Commander Defense Documentation Center ATTN: DCC-TCA Cameron Station Alexandria, VA 22314
1	Director Defense Advanced Research Projects Agency ATTN: C. R. Lehner 1400 Wilson Boulevard Arlington, VA 22209
2	Director Institute for Defense Analyses ATTN: Dr. H. Wolfhard R. T. Oliver 400 Army-Navy Drive Arlington, VA 22202
1	Commander US Army Materiel Development and Readiness Command ATTN: DRCDMA-ST 5001 Eisenhower Avenue Alexandria, VA 22333
1	Commander US Army Aviation Systems Command ATTN: DRSAV-E 12th and Spruce Streets St. Louis, MO 63166
1	Director US Army Air Mobility Research and Development Laboratory Ames Research Center Moffett Field, CA 94035
1	Commander US Army Electronics Command ATTN: DRSEL-RD Ft. Monmouth, NJ 07703
1	Commander US Army Missile Command ATTN: DRSMI-R Redstone Arsenal, AL 35809
1	Commander US Army Tank Automotive Development Command ATTN: DRDTA-RWL Warren, MI 48090
2	Commander US Army Mobility Equipment Research & Development Command ATTN: Tech Doc Ctr, Bldg 315 DRSME-RZT Ft. Belvoir, VA 22060
1	Commander US Army Armament Command Rock Island, IL 61202
3	Commander US Army Frankford Arsenal ATTN: SARFA-PDC, Dr. Lannon SARFA-MDS, Mr. Dickey SARFA-MDP-R, Mr. Stiefel Philadelphia, PA 19137
2	Commander US Army Picatinny Arsenal ATTN: SARPA-FR-G, Dr. J. Picard SARPA-FR-G, Mr. C. Lenchitz Dover, NJ 07801
1	Commander US Army White Sands Missile Range ATTN: STEWS-VT WSMR, NM 88002
1	Commander US Army Watervliet Arsenal ATTN: R. Thierry/Code SWEWV-RD Watervliet, NY 12189
1	Commander US Army Harry Diamond Labs ATTN: DRXDO-TI 2800 Powder Mill Road Adelphi, MD 20783

DISTRIBUTION LIST

No. of Copies	Organization
1	Commander US Army Materials and Mechanics Research Center ATTN: DRXMR-ATL Watertown, MA 02172
1	Commander US Army Natick Research and Development Command ATTN: DRXRE, Dr. D. Sieling Natick, MA 01762
1	Director US Army TRADOC Systems Analysis Activity ATTN: ATAA-SA WSMR, NM 88002
1	Commander US Army Research Office ATTN: Tech Lib P.O. Box 12211 Research Triangle Park, NC 27706
1	Chief of Naval Research ATTN: Code 473 800 N. Quincy Street Arlington, VA 22217
1	Commander US Naval Sea Systems Command ATTN: J. W. Murrin (NAVSEA-0331) National Center, Bldg 2, Rm 6E08 Washington, DC 20360
2	Commander US Naval Surface Weapons Center ATTN: S. J. Jacobs/Code 240 Code 730 Silver Spring, MD 20910
1	Commander US Naval Surface Weapons Center ATTN: Tech Lib Dahlgren, VA 22338
1	Commander US Naval Underwater Systems Center Energy Conversion Department ATTN: R. S. Lazar/Code 5B331 Newport, RI 02840
2	Commander US Naval Weapons Center ATTN: Dr. R. Derr Mr. C. Thelen China Lake, CA 93555
1	Commander US Naval Research Laboratory ATTN: Code 6180 Washington, DC 20375
3	Superintendent US Naval Postgraduate School ATTN: Tech Lib Dr. David Netzer Dr. Allen Fuhs Monterey, CA 93940
2	Commander US Naval Ordnance Station ATTN: Dr. A. Roberts Tech Lib Indian Head, MD 20640
2	AFOSR ATTN: J. F. Masi Dr. B. T. Wolfson Bolling AFB, DC 20332
2	AFRPL (DYSC) ATTN: Dr. D. George Mr. J. N. Levine Edwards AFB, CA 93523

DISTRIBUTION LIST

No. of Copies	Organization
1	Lockheed Palo Alto Rsch Labs ATTN: Tech Info Ctr 3251 Hanover Street Palo Alto, CA 94304
1	Aerojet Solid Propulsion Co. ATTN: Dr. P. Micheli Sacramento, CA 95813
1	ARO Incorporated ATTN: Mr. N. Dougherty Arnold AFS, TN 37389
1	Atlantic Research Corporation ATTN: Dr. M. K. King 5390 Cherokee Avenue Alexandria, VA 22314
1	AVCO Corporation AVCO Everett Research Lab Div ATTN: D. Stickler 2385 Revere Beach Parkway Everett, MA 02149
2	Calspan Corporation ATTN: Dr. E. B. Fisher A. P. Trippe P.O. Box 235 Buffalo, NY 14221
1	ENKI Corporation ATTN: M. I. Madison 9015 Fulbright Avenue Chatsworth, CA 91311
1	Foster Miller Associates, Inc. ATTN: A. J. Erickson 135 Second Avenue Waltham, MA 02154
1	General Electric Company Armament Department ATTN: M. J. Bulman Lakeside Avenue Burlington, VT 05402
1	General Electric Company Flight Propulsion Division ATTN: Tech Lib Cincinnati, OH 45215
1	Paul Gough Associates, Inc. ATTN: Dr. P. S. Gough P.O. Box 1614 Portsmouth, NH 03801
2	Hercules Incorporated Alleghany Ballistic Lab ATTN: Dr. R. Miller Tech Lib Cumberland, MD 21501
2	Hercules Incorporated Bacchus Works ATTN: Dr. M. Beckstead Dr. R. Simmons Magna, UT 84044
1	IITRI ATTN: Dr. M. J. Klein 10 West 35th Street Chicago, IL 60615
1	Olin Corporation Badger Army Ammunition Plant ATTN: J. Ramnarace Baraboo, WI 53913
2	Olin Corporation New Haven Plant ATTN: R. L. Cook D. W. Riefler 275 Winchester Avenue New Haven, CT 06504
1	Physics International Company ATTN: J. D. Watson 2700 Merced Street Leandro, CA 94577

DISTRIBUTION LIST

No. of Copies	Organization
1	Pulsepower Systems, Inc. ATTN: L. C. Elmore 815 American Street San Carlos, CA 94070
1	R&D Associates ATTN: Dr. R. B. Edelman P.O. Box 9695 Marina del Rey, CA 90291
2	Rockwell International Corp. Rocketdyne Division ATTN: Dr. C. Obert Dr. J. E. Flanagan 6633 Canoga Avenue Canoga Park, CA 91304
2	Rockwell International Corp. Rocketdyne Division ATTN: Mr. W. Haymes Tech Lib McGregor, TX 76657
1	Shock Hydrodynamics, Inc. ATTN: Dr. W. H. Anderson 4710-16 Vineland Avenue North Hollywood, CA 91602
1	Thiokol Corporation Elkton Division ATTN: E. Sutton Elkton, MD 21921
3	Thiokol Corporation Huntsville Division ATTN: Dr. D. Flanigan Dr. R. Glick Tech Lib Huntsville, AL 35807
2	Thiokol Corporation Wasatch Division ATTN: Dr. John Peterson Tech Lib P.O. Box 524 Brigham City, UT 84302
1	TRW Systems Group ATTN: Dr. H. Korman One Space Park Redondo Beach, CA 90278
1	Ultrasystems, Inc. President's Office ATTN: T. J. Tyson 500 Newport Center Drive Newport Beach, CA 92660
2	United Technology Center ATTN: Dr. R. Brown Tech Lib P.O. Box 358 Sunnyvale, CA 94088
1	Universal Propulsion Co. ATTN: H. J. McSpadden P.O. Box 546 Riverside, CA 92502
1	Battelle Memorial Institute ATTN: Tech Lib 505 King Avenue Columbus, OH 43201
1	Brigham Young University Dept of Chemical Engineering ATTN: Prof. R. Coates Provo, UT 84601
1	California Institute of Tech Jet Propulsion Laboratory ATTN: Prof. F. E. C. Culick Pasadena, CA 91103
1	Case Western Reserve Univ. Division of Aerospace Sciences ATTN: Prof J. Tien Cleveland, OH 44135

DISTRIBUTION LIST

No. of Copies	Organization
3	Georgia Institute of Technology School of Aerospace Engineering ATTN: Prof B. T. Zinn Prof E. Price Prof W. C. Strahle Atlanta, GA 30332
1	Johns Hopkins University Applied Physics Laboratory Chemical Propulsion Information Agency ATTN: Mr. T. Christian Johns Hopkins Road Laurel, MD 20810
1	Massachusetts Institute of Technology Dept of Mechanical Engineering ATTN: Prof. T. Toong Cambridge, MA 02139
1	Pennsylvania State University Applied Research Lab ATTN: Dr. G. M. Faeth P.O. Box 30 State College, PA 16801
1	Pennsylvania State University Dept of Mechanical Engineering ATTN: Prof. K. Kuo University Park, PA 16801
3	Princeton University Forrestal Campus Library ATTN: Prof M. Summerfield Dr. L. Caveny Tech Lib P.O. Box 710 Princeton, NJ 08540
2	Purdue University School of Mechanical Engineering ATTN: Prof. J. Osborn Prof. S. N. B. Murthy TSPC Chaffee Hall West Lafayette, IN 47906
1	Rutgers State University Dept of Mechanical and Aerospace Engineering ATTN: Prof. S. Temkin University Heights Campus New Brunswick, NJ 08903
1	Southwest Research Institute Fire Research Section ATTN: W. H. McLain P.O. Drawer 28510 San Antonio, TX 78228
1	Stanford Research Institute Propulsion Sciences Division ATTN: Tech Lib 333 Ravenswood Avenue Menlo Park, CA 94024
1	Stevens Institute of Technology Davidson Laboratory ATTN: Prof. R. McAlevy III Hoboken, NJ 07030
1	University of California, San Diego AMES Department ATTN: Prof. F. Williams P.O. Box 109 La Jolla, CA 92037
1	University of Illinois Dept of Aeronautical Engineering ATTN: Prof. H. Krier Transportation Bldg, Rm 105 Urbana, IL 61801
1	University of Minnesota Dept of Mechanical Engineering ATTN: Prof. E. Fletcher Minneapolis, MN 55455
2	University of Utah Dept of Chemical Engineering ATTN: Prof. A. Baer Prof. G. Flandro Salt Lake City, UT 84112

DISTRIBUTION LIST

Aberdeen Proving Ground

Marine Corps Ln Ofc
Dir, USAMSAA